On the detection of the solar signal in the tropical stratosphere

G. Chiodo[1], D.R.Marsh[2], R.Garcia-Herrera[1,3], N.Calvo[1], and J.A. García[4]

[1]Universidad Complutense de Madrid, Spain
[2]National Center for Atmospheric Research, Boulder (CO), USA
[3]Instituto de Geociencias (IGEO), Madrid, Spain
[4]Universidad de Extremadura, Badajoz, Spain

Correspondence to: Gabriel Chiodo
gchiodo@ucm.es

Abstract. We investigate the relative role of volcanic eruptions, El-Niño Southern-Oscillation (ENSO) and the Quasi-Biennal-Oscillation (QBO) in the quasi-decadal signal in the tropical stratosphere in temperature and ozone commonly attributed to the 11 yr solar cycle. For this purpose, we perform transient simulations with the Whole Atmosphere Community Climate Model forced from

5 1960 to 2004 with an 11 yr solar cycle in irradiance and different combinations of other forcings. An improved multiple linear regression technique is used to diagnose the 11 yr solar signal in the simulations. One set of simulations includes all observed forcings, and is thereby aimed at closely reproducing observations. Three idealized sets exclude ENSO variability, volcanic aerosol forcing, and QBO in tropical stratospheric winds, respectively. Differences in the derived solar response in

10 the tropical stratosphere in the four sets quantify the impact of ENSO, volcanic events and the QBO in attributing quasi-decadal changes to the solar cycle in the model simulations. The novel regression approach shows that most of the apparent solar-induced lower stratospheric temperature and ozone increase diagnosed in the simulations with all observed forcings is due to two major volcanic eruptions (i.e., El Chichón in 1982 and Mt. Pinatubo in 1991). This is caused by the alignment of these

15 eruptions with periods of high solar activity. While in the middle and upper tropical stratosphere, it is feasible to detect a robust solar signal, this is not the case in the tropical lower stratosphere, at least in a 45 yr simulation. The present results suggest that in the tropical lower stratosphere, the portion of decadal variability that can be unambigously linked to the solar cycle may be smaller than previously thought.

1 Introduction

The sun climate connection is a topic of high relevance since solar variability is one source of natural variability in the climate system. The 11 yr solar cycle is a well documented mode of variation of solar activity. To date, observations show decadal variations in the climate system, that are commonly attributed to the 11 yr solar cycle (see review by *Gray et al.*, 2010). A well established

25 decadal variability can be found in reanalysis data of stratospheric temperature (*Crooks and Gray*, 2005). An extended reanalysis dataset from ECMWF seems to confirm this pattern (*Frame and Gray*, 2010). A similar variability has also been found in stratospheric ozone in three independent satellite datasets (*Soukharev and Hood*, 2006).

In the tropical stratospheric domain (25° N–25° S), these studies show that zonal mean tempera-

30 ture and ozone vary in phase with solar activity (i.e., a warming and an ozone increase are found during peaks in solar activity). The vertical structure of the observed positive response is composed of a double peak, with maxima in the upper stratosphere at 1–3 hPa and tropical lower stratosphere (hereafter TLS) at 50–70 hPa, along with a minimum response in the middle stratosphere at 10–20 hPa (e.g., see Fig. 1 in *Frame and Gray*, 2010, for temperature, and Fig. 5 in *Soukharev and*

35 *Hood*, 2006). While the upper stratospheric peak is well established and in agreement with theoretical expectations, the structure of the signal in the middle stratosphere and TLS is more uncertain, and far less understood. It has been suggested that a solar cycle modulation of tropical upwelling may be the dynamical mechanism originating the response in the TLS in ozone (*Hood*, 1997; *Hood and Soukharev*, 2003) and temperature (*Kodera and Kuroda*, 2002). However, this mechanism is

40 linked to changes in wave-driving of extratropical circulation, and it is mainly operative in the winter stratosphere, where the strong variability therein makes the detection of such changes extremely challenging.

Chiodo et al. (2012) reported good agreement in the simulated vertical profile of the solar signal from the Whole Atmosphere Community Climate Model (WACCM), version 3.5, and observations.

45 WACCM3.5 is a general circulation model with a well resolved stratosphere and interactive chemistry. Reasonable agreement was also found in other models of similar characteristics (*Austin et al.*, 2008; *Schmidt et al.*, 2010). However, the ability of the models in reproducing the signal in the TLS appears to depend on the boundary conditions, and the elements necessary to reproduce such a signal are model dependent. For this reason, the role of additional sources of variability (e.g., ENSO, or

50 QBO in those models which assimilate it) in the tropical lower stratospheric solar signal is far from being understood. The detection of solar signals is also difficult considering their relatively small amplitude compared with other sources of variability. This is especially true in the TLS, where a substantial portion of interannual variability is controlled by the QBO in both ozone (*Randel and Wu*, 2007) and temperature (*Randel et al.*, 2009b). Another important driver for interannual variability in

55 the TLS is ENSO (*Calvo-Fernández et al.*, 2004; *Randel et al.*, 2009a). Volcanic eruptions also lead to strong temperature and ozone changes in this region, where decreases of 5–10 % in ozone and

a warming of more than 1 K after the Mt. Pinatubo eruption in 1991 were reported (*Randel et al.*, 1995).

Solar signals in observations and transient simulations are usually quantified with multiple linear regression (MLR) models that include a linear trend term, and proxies for ENSO, QBO, and volcanic eruptions. Unambiguous attribution using a MLR model requires the predictors to be orthogonal (i.e., that they are not cross-correlated), and predictand time series to be serially uncorrelated. However, serial correlation in temperature and ozone exists within seasonal time scales (*Tiao et al.*, 1990). Additionally, cross correlations between proxies may arise during certain epochs. This is the case for the QBO, which is characterized as the vertical profile of the equatorial zonal mean zonal wind. The zonal wind in the tropical stratosphere can potentially be affected by ENSO and in-situ heating caused by volcanic aerosol. Thus, volcanic and ENSO signals are embedded in the QBO index. Hence, deviations from the basic assumptions limit the reliability of estimates from regression models, especially when using data that only cover a few solar cycles, as in the case of reanalysis and satellite datasets.

The only feasible approach to quantify aliasing in observational data is to assess the sensitivity of the derived solar regression coefficients to the formulation of the regression model. This is the method used by some authors (*Frame and Gray*, 2010; *Soukharev and Hood*, 2006; *Hood et al.*, 2010), who claimed that their solar regression coefficient is clean from aliasing because of the very small changes when including ENSO, QBO, and volcanic terms in their regression model.

On the other hand, when using a climate model, the sensitivity of the simulated solar signal to the presence of other boundary conditions can be directly tested. This was done in simulations with a 2-D chemistry transport model (*Smith and Matthes*, 2008; *Lee and Smith*, 2003). *Smith and Matthes* (2008) showed that the simulated solar signal in tropical ozone strongly depends on the presence of the QBO. They showed that this dependence is indicative of a contamination of the solar signal by the QBO, and that the aliasing is mainly due to irregularities (i.e., departures from a sinusoidal function) in the observed QBO. In an earlier study using the same 2-D model, *Lee and Smith* (2003) found that volcanic eruptions have a similar effect, and that both QBO and volcanic signals equally alias on the observed structure of the ozone solar response. However, one may argue that such simplified 2-D models lacked a full description of wave-mean flow interactions that have been proposed to explain the origin of the decadal changes in the TLS.

Marsh and Garcia (2007) used a more comprehensive model to investigate tropical ozone decadal variability (WACCM3.1, *Garcia et al.*, 2007). They found that the ozone solar signal in the TLS could only be reproduced by WACCM3.1 when observed SSTs were prescribed. They demonstrated that part of the ozone solar signal simulated in transient WACCM simulations was due to spurious correlation between the index for the solar cycle and ENSO over the 1979–2003 period. These conclusions were obtained by contrasting transient WACCM3.1 simulations performed with observed SSTs with time-slice experiments performed with climatological SSTs. Nevertheless, neither of

these simulations included the radiative effects of volcanic eruptions, or a QBO. Thus, their results cannot be directly compared to observations.

There is clearly a need for a quantitative estimate of the portion of the decadal signals in the stratosphere which can unambiguously be linked to the solar cycle. It has been demonstrated that a warming in the TLS, such as that commonly attributed to the solar cycle, can trigger changes in tropospheric circulation (*Haigh and Blackburn*, 2006). Consequently, a correct attribution of changes in the TLS may in turn improve our understanding of the role of external forcings on tropospheric and surface climate that propagate downward from the stratosphere.

In this paper, we quantify the impact of the presence of other forcings on the detection of the 11 yr solar cycle signal in simulations of the WACCM3.5 version including more realistic forcing than in previous studies. WACCM3.5 is a valuable tool for this exercise, since it was previously shown that this model version is able to reproduce most features of the apparent 11 yr solar cycle observed in the tropical stratosphere over the last several decades (*Chiodo et al.*, 2012).

We compare the amplitude of the solar signal in simulations with all observed forcings to those where a single forcing has been excluded. Differences between the simulations quantify the impact of the exclusion of each forcing on the apparent solar signal, and thus the potential aliasing from the respective sources. The solar signal is diagnosed using a novel MLR approach, which reduces the autocorrelation and improves the accuracy of the regression fit through the use of an optimal lag in the predictors.

The paper is arranged as follows. Section 2 provides a description of the model and the experimental setup, along with the statistical methods employed in the analysis. The results are outlined in Sect. 3. Section 3.1 is dedicated to the relationship between each forcing and the simulated temperature and ozone variations. Focus is then given on the 11 yr solar cycle signal in Sect. 3.2. The robustness of the apparent solar signal in the reference case is assessed in Sect. 3.3. A generic discussion of the results and their implications is given in Sect. 4, while Sect. 5 summarizes the main results and conclusions.

2 Data and methodology

2.1 Model simulations

WACCM3.5 is an improved version of the WACCM3.1 general circulation model (*Garcia et al.*, 2007). The standard resolution of 66 vertical levels ranging up from the surface to the thermosphere (140 km), and $1.9°$ latitude by $2.5°$ longitude in the horizontal was used in this work. This is the same model version that participated in the CCMVal-2 activity (*CCMVal-2*, 2010). Details of the model relevant for simulating the 11 yr solar cycle are discussed in *Chiodo et al.* (2012).

We performed pairs of simulations of WACCM3.5 model run from 1960 to 2004. The set-up of one pair is identical to the REFB1 type of simulations presented in *Eyring et al.* (2010) for

4

a comparison with other Chemistry Climate Models and in *Chiodo et al.* (2012) for a detailed
analysis of the 11 yr solar cycle signal. It is named here as "all forcings" due to the inclusion of
all known natural and anthropogenic forcings. The forcings include observed SSTs and sea-ice
concentrations (*Hurrell et al.*, 2008), loadings of GHG and ozone depleting substances. Model
equatorial stratospheric winds are relaxed toward observed winds to obtain a realistic time-varying
QBO (*Matthes et al.*, 2010). The effects of volcanic eruptions are included by prescribing aerosol
surface area densities (SAD), compiled from a combination of Stratosphere Aerosol and Gas Ex-
periment (SAGE) measurements (*Thomason et al.*, 1997) and Solar Mesosphere Explorer (SME)
instruments from 1979 onward. Aerosol data before 1979 are constructed based on assumptions of
background aerosol (*CCMVal-2*, 2010). The impact on the heating rates in the stratosphere is ex-
plicitly calculated (*Tilmes et al.*, 2009). The 11 yr solar cycle in solar irradiance is introduced in the
model by prescribing spectral irradiance data modeled by *Lean et al.* (2005), integrated over specific
model bands for radiation and chemistry calculations. This set of simulations is aimed at closely
reproducing observed interannual variations in the tropical stratosphere, and serves as a reference
case.

In the second set of experiments, named "fixedSSTs", a climatological seasonal cycle of the SSTs
is prescribed, thus removing ENSO from possible sources of variability in the stratosphere. In the
next set called "noQBO", the tropical stratospheric winds are not relaxed towards observations.
Since the model version used in this work does not spontaneously generate a QBO, permanent weak
easterlies in the tropical stratosphere are simulated. Finally, the fourth set named "noVOLC" is
forced with a constant seasonal cycle of SAD, thus excluding peaks in sulfate aerosol concentrations
in the stratosphere due to volcanic eruptions. The list of experiments is given in Table 1.

2.2 Analysis method

Monthly mean output is averaged over the two realizations done for each of the four sets, season
(DJF, MAM, JJA, SON), longitude, and the $25°$ N–$25°$ S latitude band. The tropical average seasonal
mean anomalies are used as input for an improved MLR technique, whose formulation is novel in
the context of solar cycle studies. Details are described in the Appendix and are briefly outlined
below.

First, the autocorrelation is removed following a Box-Jenkins pre-whitening procedure (*Box and
Jenkins*, 1980). This is applied on the time series of the seasonal means of the simulated ozone
and temperature and of the predictors (i.e., the forcings used in each set). Next, lags are calculated
that maximize the absolute value of the correlation between the prewhitened field variable and the
forcings. In this way, the projection of the field variable onto the forcings in each set is maximized.
These steps have been extensively used in the formulation of multiple linear regression models in
other fields (e.g. in biometeorology, *Diaz et al.*, 2002a,b and economic forecasting, *Bisgaard and
Kulahci*, 2011), though they are new in the analysis of the 11 yr solar signal.

5

165   The suitable lag for each predictor must be chosen with care. Ideally, the lag correlations should represent a physically consistent relationship between the predictand and predictors. On the other hand, such lags should not bring different predictors into phase, thereby increasing collinearity. With these criteria in mind, an optimal window, over which the suitable lag is searched for, is identified.

     In our analysis, we use zonal wind time series at 30 and 10 hPa, which serve as QBO indices in

170   the regression. By using the residual of a regression of the zonal wind onto other indices, the QBO indices become orthogonal to the other predictors. We exclude any lags in the QBO term itself in order to keep the mutual phase relationship in both indices (see Appendix). We find that by using this technique, the cross correlation among the QBO indices and the other predictors never exceeds 0.06, which ensures that the null-hypothesis of no correlation cannot be rejected at the 99 % confidence

175   level.

     Principal component analysis (PCA) has been used in previous studies to derive orthogonal QBO indices (*Randel and Wu*, 1996; *Crooks and Gray*, 2005; *Frame and Gray*, 2010). The mathematical orthogonality constraint can potentially limit the physical realism of the principal component associated with the QBO. For this reason, we believe that the residuals from a MLR at 30 and 10 hPa are

180   more directly linked to the original wind field at both heights, and thus more suited than principal components for representing the QBO variability in the MLR.

     This procedure is repeated for each of the simulation sets, to both temperature and ozone. The regression model formulated in Eq. (A6) is applied at constant pressure levels of the tropical stratospheric domain (0.1–100 hPa).

185   The MLR includes only predictors for those forcings included in the specific set of experiments (e.g. no QBO term is used in the analysis of the "noQBO" set). Since the main focus of this paper is the detection of the solar signal in the tropical stratosphere, results from the regression analysis are only presented for the UV coefficient (β'_{uv} in Eq. A6). The coefficient has been scaled at all isobaric levels by 0.175. This scaling factor is the 2σ value of the UV radiation index used in the MLR,

190   which represents the peak to trough solar cycle variation in units $\mathrm{W\,m^{-2}\,nm^{-1}}$.

3   Results

Figure 1 shows the time series of the tropical average (25° N–25° S) seasonal mean anomalies of the zonal mean temperature at the 50 hPa level from the "all forcings" set. A long-term cooling trend is evident, and the amplitude of approximately -0.5 K per decade agrees with observations (*Randel*

195   *et al.*, 2009b). The trend is interrupted by positive peaks over 2 K in 1964 and 5 K in 1992, which are caused by two major volcanic eruptions; i.e., Agung and Mt. Pinatubo. Among these events, the Mt. Pinatubo eruption is the best characterized eruption on records. These records show a 1-2 K warming in 1992 in the 50 hPa global mean (*Randel et al.*, 2009b), while anomalies over the tropical belt reach 3 K (see Fig.1 in *Tilmes et al.*, 2009). Compared to these values, WACCM tends

200   to overestimate the heating caused by the sulfate aerosols associated with the Mt. Pinatubo eruption.

Before applying the MLR, the variables and the forcings are prewhitened with the autocorrelation coefficient of the field variables. Since the choice of the lag for the predictors is crucial to improve the regression fit, we first analyze the lag correlation between forcings and the simulated field variables temperature and ozone.

205   ## 3.1   Lag correlation analysis

The optimal lag must ensure a physically consistent relationship between the prewhitened field variables and the forcings. For this purpose, the vertical structure of the lag correlation is analysed in detail, in order to identify a window representing a realistic time-scale for the response in the selected variable to each of the applied forcings.

210   Figure 2 shows the vertical profile of the correlation of the tropical average seasonal mean temperature with UV radiation from the "all forcings" set, plotted as a function of the time lag in a window of 10 yr (-5 to $+5$), thus covering an almost complete solar cycle. Correlations at positive lag values mean that variations in UV lead temperature changes. Although the pre-whitening of the time series considerably reduces the magnitude of the correlations, a well defined positive temperature-UV

215   relation is found at 1 hPa, which lingers for 2 yr around the peak of solar activity (that is, from lag -1 yr to 1 yr). Negative values can be seen 5 yr prior and after the peak in UV radiation, indicating a cooling around minima of solar activity. Between 10 and 70 hPa, we identify positive maxima at lags of 0.75, 1.75 and 3.25 yr. Among them, the peak at 0.75 yr corresponding to 3 seasons (or 9-11 months) seems to be connected to the upper stratosphere. This suggests that the warming induced

220   by maxima in solar activity is instantaneous and longer-lasting in the upper stratosphere, whereas it is slightly weaker and delayed by a few seasons in lower layers.

Overall, the lag correlation to the UV in the WACCM simulations depicts a downward propagation of the solar signal. This is consistent with the "top-down" mechanism involving a downward pathway (which is thus mediated by the stratosphere) for solar influences to impact surface climate,

225   as hypothesized in previous studies (*Meehl et al.*, 2009; *Gray et al.*, 2010). The broad time span of the maximum at 1 hPa is most likely due to absorption of UV radiation whose peaks, on average over the recorded 11 yr cycles 19-23, last for about 2-3 years (*Lean et al.*, 2005). In lower levels, the intermittency of the positive correlations suggests a seasonality in the apparent downward propagation of the temperature signal. One candidate mechanism for such propagation is the strengthening of the

230   wintertime polar night jet during solar maxima, which causes suppressed tropical upwelling (*Kodera and Kuroda*, 2002). This mechanism is captured by WACCM (*Chiodo et al.*, 2012), and the time scales for the downward propagation are consistent with the lags found in the positive correlations of the 0-1 yr window.

The lag correlation of UV radiation with tropical mean ozone is shown in Fig. 3. As it occured

235   in zonal mean temperature, a broad structure of positive ozone-UV correlations appears around lag

7

0 in the upper stratosphere (0.1-10 hPa), with two peaks at 1 and 5 hPa. A more complex structure in the lag correlations is found in lower levels. At 10-50 hPa, there is a small region with negative values around lag 0, while positive correlations appear at lags of 0.75-1 yr. At 50-100 hPa, positive correlations are found between 0-1 yr, maximizing at a lag of 0.25 yr, equal to 1 season. Except for the negative correlations at 30 hPa, there is good correspondence between temperature and ozone in the 0-1 yr window.

The in-phase ozone-UV relationship in the middle and upper stratosphere is likely due to the UV-induced photolysis of molecular oxygen, and recombination with atomic oxygen (*Pap and Fox*, 2003). This process is instantaneous, and extends for the 2-3 years of peak solar activity. As in temperature, the intermittency in the correlations at lower levels suggests a seasonality in the lower stratospheric ozone response. In the 0-1 yr span, the correspondence in the temperature and ozone correlations suggests that the same mechanism is controling ozone and temperature responses in this window. Unlike in temperature, there is less evidence of a delayed response at lags larger than 1 yr throughout the 30–100 hPa region. This indicates that at such lags, it is difficult to link both temperature and ozone responses through a common mechanism.

Once we have analyzed the structure of the correlations, we next identify the optimal lag which maximizes the absolute value of the cross correlation with the UV index. We constrain the window over which the optimal lag is identified to the 0-1 yr time span, motivated by the finding that a coherent variation in correlations with temperature and ozone was present in that interval. An added benefit of limiting the lag in the 0 to 1 yr window is that the cross correlation between the UV index and the other predictors is minimized. Hence, the optimal UV lag (τ_{uv}) to be used in Eq. (A6) is chosen in this window.

The vertical profile of τ_{uv} is shown in Fig. 4 for zonal mean temperature and ozone. We show the values obtained for the "all forcings" case (a), and for the three idealized sets (b–d). Overall, the temperature-UV and the ozone-UV correlation patterns are found to be qualitatively similar in the three simulation sets excluding single forcings (not shown), which explains the similarity in the vertical profile of the optimal lag. In the case of zonal mean temperature, the profile shows a downward progression in all four cases, with a lag of 0.5 yr (or 2 seasons) at 10 hPa, 0.75 yr (or 3 seasons) between 20 and 70 hPa, and 1 yr between 80 and 100 hPa, consistent with the lagged positive correlation in this region seen in Fig. 2. In tropical ozone, the lag needed to maximize the correlation in the TLS is slightly smaller than in temperature, as seen in Fig. 3.

We also analyzed the lag correlation for the other terms included in Eq. (A6); the two QBO indices, N3.4 and SAD. As the present paper is focused on the solar response, we discuss it without showing additional Figures. The cross correlation of temperature and ozone with $u30'$ and $u10'$ shows a downward propagating pattern associated with the meridional secondary circulation of the imposed QBO (*Baldwin et al.*, 2001). For the N3.4 index, negative correlations of ozone and temperature maximize at 0.5 yr (6–8 months, or 2 seasons) and 0.25 yr (3–5 months, or 1 season)

8

respectively, consistent with the lagged impact of El Niño on the TLS through an increase in tropical upwelling (*Marsh and Garcia*, 2007; *Calvo et al.*, 2010). For the SAD index, we find positive correlations in temperature and negative values in ozone, both peaking at zero lag, and decaying as the lag increases to around 1.5 yr.

We constrained the optimal lag in the N3.4 and SAD indices to be no more than one year, as it was done for the UV index. This is motivated by the fact that at lags longer than 1 yr, spurious interference with the QBO appears in the form of downward propagating QBO structures, in both ozone and temperature correlations with N3.4 and SAD indices. Also, the cross correlation between N3.4, SAD and QBO indices in the 0 to 1 yr window is minimized. Hence, the optimal lag maximizing the correlation with these indices, (i.e., τ_{enso} and τ_{volc} in Eq. A6), is chosen in this window.

We do not use a lag for the SAD index for the regression of both temperature and ozone, as the strongest correlation is found at zero lag. This implies that in Eq. (A6), $\tau_{volc} = 0$ at all levels. For the N3.4 index, we use $\tau_{enso} = 0.25$ yr (or 1 season) for the regression of temperature, while a value of 0.5 yr (or 2 seasons) is used for ozone. No lags are used in $u10'$ and $u30'$, as the optimal fit is obtained by adjusting the relative weighting (i.e. regression coefficients) of these roughly sinusoidal variations. With these values for τ_{enso}, τ_{volc} and those for τ_{uv} displayed in Fig. 4, a regression of the time series of zonal mean wind at 10 and 30 hPa ($u10'$ and $u30'$) is performed (see Eq. (A5)). The residuals are then taken as QBO indices (i.e., $u10^*$ and $u30^*$ in Eq. (A6)).

An example of the application of the MLR procedure employed in this paper is given for the tropical average zonal mean temperature at 50 hPa, which is the time series shown in Fig. 1. Figure 5a shows the temperature time series after pre-whitening, along with the fit output from the MLR model formulated in Eq. (A6). As seen in Fig. 4, the optimal UV lag (τ_{uv}) used at this level is 0.75 yr (or 3 seasons), while τ_{enso}=0.25 yr (or 1 season). It is found that while the pre-whitening smooths part of the variability, the peaks of the original time series shown in Fig. 1 are preserved. The r^2 value of 0.4 implies that 40 % of the variability in the prewhitened temperature time series can be explained by the regression fit. Note that if no optimal lag is used for the predictors, the r^2 value would be 0.2 (not shown), which indicates a less accurate fit. Figures 5b–f plot the contribution of each term on the right hand side of Eq. (A6) to the regression fit shown in Fig. 5a. The strongest temperature changes are caused by volcanic eruptions, with Mt. Pinatubo generating a 3 K anomaly (Fig. 5f). Changes of 0.5–1 K are associated with the first QBO term ($u30^*$; that is, the filtered zonal wind at 30 hPa) and ENSO (Fig. 5c–d). On the other hand, the 11 yr solar cycle signal is smaller, with temperature deviations of a few tenths of a K (Fig. 5b).

3.2 The 11 yr solar cycle signal

The vertical profile of the solar signal, shown as the UV regression coefficient (β'_{uv}) of the tropical average ($25°$ N–$25°$ S) zonal mean temperature scaled by 2σ of UV radiation (0.175), is shown in Fig. 6. The profile is shown for the reference "all forcings" set, and the idealized experiments, using

the optimal lag for the UV index shown in Fig. 4.

310   In the "all forcings" set (black line in Fig. 6), a statistically significant UV-induced warming is found throughout the tropical stratosphere, with maximum values of 0.8 K at 1 hPa and a secondary maximum of 0.6–0.7 K at 40–50 hPa. It is interesting to note that a statistically significant solar signal is also extracted in the middle stratosphere at 10 and 20 hPa, even though this is a region of relative minimum response. The lag used for the UV index is 0 at 1 hPa, 6–8 months (or 2 seasons)

315   at 10 hPa, and 9–11 months (or 3 seasons) between 20 and 70 hPa (see Fig. 4).

       In the "fixedSSTs" case (red line in Fig. 6), the simulated temperature solar signal is similar to the reference case, although the secondary maximum at 50 hPa is obtained at a slightly larger lag compared to the other sets ($\tau_{uv} = 1$ yr, see Fig. 4). The strong similarity in the derived UV regression coefficient in temperature suggests that the ENSO contribution to the apparent solar signal

320   is negligible. The low sensitivity of the UV regression coefficient to the inclusion of ENSO is not due to the removal of the serial correlation, as similar results are obtained without pre-whitening the data (not shown). The "noQBO" set (green line in Fig. 6) shows a significant solar response throughout the stratosphere above 60 hPa, with a peak of 0.7 K at 50 hPa. Overall, this profile resembles the reference "all forcings" case, although a slighly stronger magnitude of the warming is evident at 50

325   hPa. In the "noVOLC" set (blue line), a significant regression coefficient is obtained at all levels above 20 hPa, with a peak of 0.7 K at 1 hPa. However, below 20 hPa the signal becomes weak and not statistically significant. Thus, no robust solar response in temperature is obtained in the TLS in the WACCM simulations that do not include volcanic eruptions. The absence of response indicates that the apparent lagged temperature solar signal in the TLS diagnosed in all other simulation sets is

330   associated with the effect of volcanic aerosols.

       For comparison, the UV coefficient was also estimated from a standard MLR (β_{uv} in Eq. (A1)). Figure 7 shows the vertical profile scaled by 0.175. The temperature response in the upper strato- sphere between 1-5 hPa is very similar to that obtained with the new technique (Fig. 6); that is, a significant warming of 0.6-0.8 K in all experiments. In the lower layers, there is less agreement

335   between the ensembles. A secondary maximum is evident in the "all forcings" and "fixedSSTs" sets, with a peak of 0.4-0.5 K at 50 hPa. A similar response is also seen in the "noQBO" set, al- though the region of statistical significance is limited to higher altitudes (20 hPa). Below 30 hPa, no significant response is seen in the "noVOLC" and "noQBO" ensembles. Comparing both tech- niques (i.e., Figs. 7 and 6) it is evident that the secondary maximum in the TLS extracted from the

340   new regression technique, when statistically significant (i.e.; in the "all forcings" and "fixedSSTs" sets), is stronger in magnitude than when using the standard MLR. Also, the new technique yields a secondary maximum in the "noQBO" set, whereas no response is seen in the standard MLR. Thus, in the TLS region the new regression method allows for better separation of the temperature solar signal from the QBO. The new method also shows a stronger reduction of the solar signal in the

345   "noVOLC" set.

The new method was also applied on the tropical mean ozone mixing ratio. The vertical profile of β'_{uv} scaled by 0.175 is shown in Fig. 8 in terms of relative solar cycle (%) peak to trough change in the mixing ratio using the lag values for the UV index shown in Fig. 4. In the "all forcings" case, there is a well defined double peak structure, with statistically significant ozone increase in the middle and

350 upper stratosphere peaking at 2 % at 10 hPa, a relative minimum at 30 hPa, and a significant increase at 40 hPa and below, peaking at 3.5 % between 70 and 90 hPa.

Fairly good agreement across all pairs of simulations is seen in the UV-induced ozone increase of 1.5-2.0 % at 5–10 hPa, although the exact height of the maximum varies. At 20 hPa, the solar cycle ozone response in the "noVOLC" and "noQBO" case is slightly stronger than in the "all forcings"

355 case. Reasonable agreement is also evident in the weakly negative response at 30 hPa, with exception of the "noQBO" case, which shows a positive and significant ozone response of 1 %.

Significant differences are evident in the amplitude of the ozone increase in the stratospheric levels between 40 and 100 hPa. While the "all forcings" case features a significant ozone increase ranging from 2.0 % at 50 hPa to 3.5 % at 70 hPa, the response in the "noVOLC" case follows a similar profile,

360 although with lower values ranging from a non-significant 0.8 % increase at 50 hPa, to 1.5–2.0 % at 70–80 hPa. At 70 hPa and below, a different response is also observed in the "noQBO" case, where a non-significant 1.0 % ozone increase is obtained. On the other hand, the ozone response at 70–80 hPa is increased to 4.0 % in the "fixedSSTs" case, although the difference between this set and the "all forcings" pair of simulations is not statistically significant. Among all experiments, the profile of

365 β'_{uv} obtained from the "fixedSSTs" set is the one that most closely resembles the "all forcings" case in the lower stratosphere. Those calculated from the "noVOLC" and "noQBO" exhibit the largest differences to the reference case, with a weaker response throughout the lower stratosphere below 40 hPa in the "noVOLC" case, and below 70 hPa in the "noQBO" case. This suggests that part of the apparent lower stratospheric ozone signal obtained from the "all forcings" case is due to QBO

370 and volcanic aliasing, with the largest spurious contribution coming from volcanic aerosol.

Figure 9 shows the ozone UV regression coefficient obtained from a standard MLR (β_{uv} in Eq. (A1)). The ozone increase of approximately 2 % at 5 hPa is similar to the response obtained from the new technique (Fig. 8). The relative minimum at 20 hPa is statistically significant, while using the new MLR, this response is not significant and higher in altitude (30 hPa). Both techniques

375 show differences between ensembles in the region below 40 hPa, although the spread seems larger in the standard MLR. In the new MLR, the difference in the solar response between the "all forcings" and "fixedSSTs" sets at 50-70 hPa is smaller compared to the standard MLR. This indicates that the use of the new regression technique reduces the ENSO aliasing in the apparent solar response of lower stratospheric ozone. Overall, both techniques show a reduction of the solar signal below

380 30 hPa in the "noVOLC" set compared to the "all forcings" set. Accordingly, the contribution of volcanic aerosol to quasi-decadal variability of tropical lower stratospheric ozone does not depend on the type of regression analysis.

11

3.3 Sensitivity of the solar signal to the data window

The results from the idealized cases give useful information about the impact of other forcings on the
analysis. However, these simulations might not be able to reproduce non-linear interactions between
the missing forcing and the 11 yr solar cycle. The aim of this section is thus to assess aliasing in
the regression of one pair of simulations driven by the combination of forcings that most closely
resembles the real atmosphere, as is the "all forcings" case. In this way, it is possible to quantify
the potential aliasing in regressing a limited record, and in turn to infer the feasibility of extracting
a robust solar signal from the window covered by observational records. One method to accomplish
this consists of testing the sensitivity of the diagnosed signal to the length of the data.

We calculate the UV regression coefficient (β'_{uv}) from the "all forcings" set for a varying data
window, whose endpoint is the last year available in the simulations: 2004. A minimum of 10 yr
is used to cover the last solar cycle (1995–2004), and the data window is gradually extended to the
whole 45 available years, using 1 yr increments.

Figure 10 shows the estimates for tropical mean temperature, calculated at 5 different pressure lev-
els representative of the upper stratosphere (1 hPa), middle stratosphere (10 hPa), and lower strato-
sphere (30, 50, and 70 hPa), scaled by the 2σ value of the UV index. Note that the end-point value
obtained with the entire 45 yr time series is identical to that shown (on the same levels) in Fig. 6.

In the upper stratosphere at 1 hPa (Fig. 10a), a constant value of 0.8–1.0 ± 0.2 K is obtained.
One can deduce that the minimum number of years necessary for extracting a significant and stable
solar signal in temperature at 1 hPa is 10–15 yr, since the value obtained with such window is fairly
close to that calculated with the full available period of 45 yr. At 10 and 30 hPa (Fig. 10b–c), the
regression coefficient is slightly negative and not significant when less than 20 yr of data are used. It
then stabilizes to a significant positive value of 0.4 ± 0.2 K at 10 hPa and 0.5 ± 0.3 K at 30 hPa when
more than 25 yr of data are used.

At lower stratospheric levels (50 and 70 hPa, shown in Fig. 10d–e), the derived values are more
uncertain than in the upper stratosphere, as indicated by the wider error bars, and exhibit stronger
sensitivity to the window length. Broadening the data window reduces the apparent signal at 50
and 70 hPa from 1.0 ± 0.7 K with 15 yr of data to 0.2–0.5 ± 0.3 K when using the 45 yr of data.
No convergence towards a steady value is found at these levels. Thus, a stable and significant
temperature response can only be detected above 30 hPa, while a different behavior is observed
at 50 and 70 hPa, where no robust value can be extracted with the available 45 yr long record.

In addition, strong swings are evident in the middle and lower stratosphere (30, 50 and 70 hPa)
a few years after the occurrence of the two major volcanic eruptions when using WACCM data,
suggesting that volcanic and solar signals cannot be cleanly separated by the regression model at
these levels. Interestingly, both Mt. Pinatubo and El Chichón eruptions appear to interfere with the
solar signal at 30 and 50 hPa. This is not the case at 70 hPa, where only the former has a discernible
impact (Fig. 10e). There are also perturbations of negative sign when the Agung eruption (1963) is

420 included in the analysis. This effect is seen at 50 hPa and 70 hPa, although the jumps are much less evident than in the case of the other two eruptions. Overall, the peaks associated with Mt. Pinatubo and El Chichón disappear after 30 yr of data are included in the regression analysis. Even when the analysis is extended using a longer window, the UV coefficient decreases at both levels, which is particularly evident at 70 hPa. This suggests that in WACCM3.5, no robust signal in temperature can

425 be extracted in the TLS with 45 yr of simulations data.

The UV regression coefficient is also estimated with the same procedure on MERRA reanalysis data (*Rienecker et al.*, 2011), chosen here over other reanalysis products due to the larger overlap with the simulations (1979–2004). WACCM and MERRA can be directly compared by using 26 yr as the window in the "all forcings" case. At this window length, the apparent solar signals at 1

430 hPa (Fig. 10a) and 10 hPa (Fig. 10b) of 0.8 and 0.3 K in the model simulations are in excellent agreement with MERRA estimates. Since the temperature response at these heights is related to the direct response to the UV radiation, the agreement with reanalysis suggests that the model sensitivity to the 11 yr UV forcing is realistic. There is also qualitative agreement at 30 hPa (Fig. 10c) 50 hPa (Fig. 10d) and 70 hPa (Fig. 10e) in the signals of respectively 0.3, 0.5 and 0.7 ± 0.2 K. However, this

435 only applies to the 26 yr window overlapping with MERRA since, as indicated above, a decrease in the diagnosed solar signal is seen as a larger analysis period is used.

It should be recalled that the warming simulated at 50 hPa after Mt. Pinatubo in 1992 is loo large (see Fig. 1). This bias might contribute to the misattribution of quasi-decadal variability when using model data in the analysis. Accordingly, the impact on the detection of solar signals might depend

440 on the size of the underlying volcanic signature. To test this possibility, we analyze the dependence of the solar signal to data windowing in the MERRA record, bearing in mind that less stability is expected due to the shorter window compared to the WACCM simulations. Figure 11 shows the regression coefficient obtained from MERRA, calculated in the same way as in Fig. 10, plotted as a function of the 26 yr window. A robust signal is found at 1 hPa and 10 hPa, with values of 0.9 ± 0.5 K

445 and 0.3 ± 0.2 K, respectively (Figs. 11a-b). The values at 30, 50 and 70 hPa (Figs. 11c-e) are less stable, which is in large part due to the peak coinciding with the Mt. Pinatubo eruption, especially at 50 hPa (Fig. 11d). There is also a tendency towards smaller values at these levels, as the window gets broader, although a stable value is not reached. This suggests that, as in WACCM, the solar signal extracted over the available observational record is not robust, mainly due to the heating associated

450 with the Mt. Pinatubo eruption.

Figure 12 shows the UV regression coefficient obtained from WACCM at 50 and 70 hPa, when periods after El Chichón and Mt. Pinatubo eruptions are omitted (June 1982–November 1983 and September 1991–November 1993). During such periods, the peaks in lower stratospheric temperature associated with the SAD index can be identified (see Fig. 5f). Convergence toward a constant

455 value of approximately 0.1 ± 0.3 K is obtained when more than 20 yr of data are used. However, this value is not significantly different from zero. When the same years are excluded from the MERRA

13

reanalysis data, the UV coefficient is also reduced from 0.6–0.7 ± 0.3 K to 0.2 ± 0.4 K at both 50 and

70 hPa. This indicates that when applying MLR methods on stratospheric temperature data covering

26 yr, a better separation of solar and volcanic signals can only be achieved with removal of data

460   around both El Chichón and Mt. Pinatubo eruptions. This is consistent with the absence of a signal

in the TLS in the set without volcanoes (blue line in Fig. 6). Note that the removal of the period after

the Agung eruption (1963-1964) would not alter the results (not shown), which is consistent with

the small impact of this event on the window sensitivity of the solar signal shown in Fig. 10.

The sensitivity to data windowing of the regression coefficient in zonal mean ozone simulated by

465   WACCM is shown in Fig. 13. The ozone signal is robust to the extension of the data window at

1 hPa (Fig. 13a), and a constant and significant ozone increase of 0.7 ± 0.4 % is found after 10 yr

of simulations data. At 10 hPa (Fig. 13b), positive and significant values of 2.2 ± 0.8 % are found

for all data windows, although jumps to higher values are evident when using less than 30 yr of

data. A significant positive UV coefficient is obtained at 30 hPa when using less than 15 yr of data

470   (Fig. 13c). However, this signal is not real since no significant ozone-UV relationship is obtained

with a larger data window. This is the region in which a relative minimum response in the vertical

profile is obtained in all idealized experiments, although with slightly different magnitudes (see

Fig. 8). At 30 hPa, the "noQBO" experiment showed a significant ozone increase of 0.6 % (see

Fig. 8), which suggests that QBO aliasing reduces the apparent 11 yr variation at this level.

475   At 50 and 70 hPa, a strong swing in the ozone UV response from negative to positive values

is evident in proximity of the Mt. Pinatubo eruption in 1991 (Fig. 13d–e), which is indicative of

the volcanic aliasing when regressing data of Mt. Pinatubo eruption. There is little evidence of

aliasing in the wake of the El Chichón eruption in 1982 at 50 hPa. At this level, a rather constant and

marginally significant value of 1.0–1.5 ± 1.0 % is diagnosed when more than 20 yr of data are used.

480   At 70 hPa (Fig. 13e), there is also a jump in proximity of the El Chichón eruption in 1982, although

the strongest variation is seen in the years around Mt. Pinatubo (1991). Overall, volcanic eruptions

have a stronger impact on the signal at 70 hPa than at 50 hPa, which is consistent with the larger

differences found at this level in the "noVOLC" set (Fig. 8). The error bars and the variations in the

amplitude are larger than at higher levels, which suggests that it is not feasible with the available data

485   to extract an accurate estimate for the ozone solar response at 70 hPa. Nevertheless, there is some

evidence of a trend toward a positive signal of 3.2 ± 1.8 % as all available 45 yr of data are included

in the analysis. This behavior is unlikely to be related to the Agung eruption, since the tendency in

the ozone solar signal starts at year 35; i.e., 6 years ahead of year 41 in the window, which would

correspond to the eruption year 1963.

490   Figure 14 shows the ozone UV coefficient calculated at 50 hPa and 70 hPa, when the El Chichón

and Mt. Pinatubo post eruption data are omitted following the same procedure taken for temperature.

A fairly constant value of 2.0 ± 1.5 % is obtained at 50 hPa when using more than 25 yr of data. These

numbers are not significantly different from those shown in Fig. 13d, which were calculated with

14

Mt. Pinatubo and El Chichón data retained. At 70 hPa, there is nearly no response at a window of 20–25 yr, and a positive trend towards positive values is evident when more than 35 yr of data are used. The value of $2.3 \pm 1.9\%$ obtained with the full 42 yr window is lower than the $3.2 \pm 1.8\%$, which was diagnosed without removing post eruption data (Fig. 13e). This is consistent with the reduction in the apparent solar signal obtained from the "noVOLC" experiment at this level (Fig. 8).

Overall, temperature and ozone show slightly different sensitivities to data windowing, which probably owes to the different processes controlling their variations in the tropical stratosphere. Further complication is brought by the low signal to noise ratio in ozone due to the relatively small ozone concentrations below 50 hPa. Nevertheless, both variables suggest that a robust solar signal can only be extracted using an MLR technique at upper and middle stratospheric levels.

4   Discussion

The tropical mean vertical profile of the 11 yr solar signal has been extracted from WACCM simulations using a novel MLR methodology. In the upper stratosphere, a 0.8 ± 0.2 K warming is diagnosed, which agrees with MERRA and ERA-40/ERA-Interim estimates within the levels of uncertainty (see Fig. 1 in *Frame and Gray*, 2010). A robust and statistically significant signal is extracted at 1 hPa using a 15–20 yr window, which is covered by stratospheric observational records. At 10 hPa, WACCM shows a significant warming of 0.4 ± 0.2 K obtained, whereas ERA-40 and ERA-Interim data show no significant response. This difference is possibly due to the different (longer) period analyzed in our study.

Between 30 and 70 hPa a significant warming of 0.5–0.7 ± 0.3 K is diagnosed in WACCM, which agrees with values reported from ERA-40/ERA-Interim reanalysis in *Frame and Gray* (2010). Similar numbers are also calculated from MERRA reanalysis at 30, 50 and 70 hPa using the same MLR technique over the same period (1979–2004, see Figs. 10c-e). Almost half of the temperature increase in this region is due to the use of a 1 yr lag in the UV index, since using a standard MLR without a lagged UV index, a warming of 0.3 to 0.4 ± 0.2 K is obtained (Fig. 7).

It is clear from Fig. 6 that the warming at 30 hPa and lower levels disappears in the set without volcanic forcing, which suggests that aliasing of the volcanic aerosol signal increases the apparent solar signal. Further evidence of this comes from the increase in the UV regression coefficient when the boundaries of the data window considered for regression analysis overlap the years of the Mt. Pinatubo and El Chichón eruptions (Fig. 10c–e). There is also a tendency towards smaller values of the UV regression coefficient in the lower stratosphere (50–70 hPa) as more years are added to the analysis, although no convergence towards a stable value is obtained even with a 45 yr window. This indicates that it is not feasible to extract a robust signal in this region over the recent past. The spurious contribution of volcanic aerosols to the UV regression coefficient is especially pronounced when using records covering 2 to 3 decades, as in MERRA reanalysis data (see Fig.11). Better

15

separation of solar and volcanic signals in temperature can be achieved by excluding El Chichón

530   and Mt. Pinatubo post eruption data from the analysis, since convergence toward a stable (though non-significant) signal is obtained in this way (shown in Fig. 12). Additionally, extending the observational data record to cover solar cycles without volcanic eruptions coincident with peaks of solar activity (as e.g., solar cycle 23) decreases the apparent solar-induced warming in the middle and lower tropical stratosphere. This is seen when regressing onto a 31 yr long ERA-Interim/ERA-40

535   merged dataset of 1978–2008 instead of the 23 yr long ERA-40 dataset of 1979–2001 (*Frame and Gray*, 2010; their Fig. 1).

The ozone increase of $2.0 \pm 0.7\%$ in the upper stratosphere at solar maximum in the "all forcings" WACCM simulation agrees well with SBUV and SAGE observations (*Soukharev and Hood*, 2006; *Randel and Wu*, 2007). An increase of similar magnitude is also obtained using a standard MLR

540   (Fig. 9), which is the more akin to the technique used to extract the signal in the mentioned observational studies than the new MLR formulated here. The response at these levels is robust, since it is stable over time, and it is also diagnosed in the idealized experiments. An accurate estimate can be extracted with 20–25 yr of data, which is a window covered by satellite data. A relative minimum response in tropical ozone is diagnosed in WACCM around 30 hPa. This structure resembles

545   the non-significant negative response seen at 10-20 hPa in SBUV and SAGE (*Soukharev and Hood*, 2006; *Randel and Wu*, 2007). The mismatch in the height of the relative minimum response from model and satellite estimates is due to the different formulation of the regression method, since the standard MLR yields a higher relative minimum (20 hPa, see Fig. 9).

A significant ozone increase is found in the lower stratosphere between 40 and 100 hPa, with

550   values ranging from $2.2 \pm 1.2\%$ at 50 hPa to $3.5 \pm 2.0\%$ at 80 hPa. Similar numbers have been previously reported for the same period covered by SAGE and SBUV data (see Fig. 12a in *Randel and Wu*, 2007, and Fig. 8 in *Soukharev and Hood*, 2006), although no comparison with these studies is possible below 50 hPa, as this is the lowest boundary in the available satellite data of stratospheric ozone. Idealized experiments show that ENSO aliasing in the lower stratospheric ozone signal is

555   negligible. This is due to the new MLR technique, which combines the use of lagged ENSO and UV terms, and to a sufficiently large window of 45 yr, which is in line with the findings of *Marsh and Garcia* (2007). On the other hand, it is also found that the apparent solar cycle ozone increase in the lower stratosphere is strongly influenced by volcanic aerosols and, to a lesser extent, by the presence of the QBO. Interference with volcanic eruptions is also indicated by the increase in the

560   UV regression coefficient when the data window overlaps periods shortly after Mt. Pinatubo and El Chichón eruptions (Fig. 13c–e). Our results confirm the findings from a study using a more simplified 2-D transport chemistry model that pointed to a strong contribution of the QBO and volcanic aliasing on the tropical ozone solar signal (*Lee and Smith*, 2003; *Smith and Matthes*, 2008).

We note that between 20 hPa a consistent bias is seen in both temperature and ozone related to

565   the problem of volcanic heating aliasing. Specifically, it appears that a fraction of the volcanic-

16

induced heating is misattributed to the solar cycle by the new and standard MLR techniques, thus producing warmer temperatures during solar maximum. This diabatic heating produces stronger upwelling rates in the simulations including all observed forcings compared to the set excluding volcanic forcing. Along with the chemically induced ozone depletion by the sulfate aerosols, the increased upwelling results in an ozone decrease due to the strongly positive vertical gradient in ozone mixing ratio, which the regression also attributes to the solar cycle, leading to a weaker solar-cycle ozone response relative to the set excluding volcanic aerosols. On the other hand, the spurious contribution of volcanic aliasing to the apparent solar signal in both temperature and ozone below 50 hPa is more difficult to be explained in these terms. At these levels, the simulated ozone depletion is generally much weaker than at 20-30 hPa, as e.g. it was the case of the Mt. Pinatubo eruption (see Fig 8.21 in *CCMVal-2*, 2010). Moreover, the regression fits from the new technique described in Eq. (A6) are carried independently for temperature and ozone. Thus, the misattribution of volcanically-induced ozone and temperature changes cannot be expected to have opposite sign throughout the lower stratosphere.

Chiodo et al. (2012) showed that the temperature and ozone signal in the TLS estimated is stronger and closer to observations in the WACCM3.5 model than in the WACCM3.1 version. The improvement is likely a consequence of WACCM3.1 not assimilating a QBO and the omission of volcanic aerosol heating in the simulations (*Garcia et al.*, 2007). Consequently, the QBO and volcanic signals did not map into the 11 yr solar cycle in the regression analysis of transient WACCM3.1 simulations, leading to a worse agreement compared to transient WACCM3.5 simulations. However, the better agreement with observations does not necessarily imply a better estimate of the solar signal. In conclusion, the present results suggest that either given a long enough window, or in idealized experiments excluding the spurious contribution of volcanic aerosols in the analysis, a consistent, though weaker than previously thought, solar response is diagnosed in the tropical lower stratosphere.

Finally, it is important to note in closing the caveat of excessive heating caused by the Mt. Pinatubo eruption in the TLS region (see Fig.1), although the precise size of the bias is difficult to assess as the uncertainty in the response derived from observations is not known. An excessive volcanic warming could have possibly contributed to the aliasing of the apparent solar signal. However, it must also be noted that the oversized heating could be due to errors in the SAD aerosol forcing dataset recommended by CCMVal (*Arfeuille et al.*, 2013). As such, this is a common bias in mainy CCMs (see e.g., Fig 8.21 in *CCMVal-2*, 2010). Depending on how the radiative transfer is handled, this affects the models sensitivity to volcanic aerosols to a greater or lesser degree than in WACCM. Thus, while there may be caveats in comparing modeled and observed MLR-derived attribution of decadal variability, our findings are likely not limited to WACCM.

17

600   **5   Summary**

We have investigated the attribution of quasi-decadal variations in tropical stratospheric temperature
and ozone to the 11 yr solar cycle. To do so, we perform a set of transient WACCM3.5 simulations
with different combination of forcings. The solar signal is extracted from the model simulations
using a new MLR approach, which (i) reduces the autocorrelation through pre-whitening and (ii)
605   improves the accuracy of the fit through the use of an optimal lag. Results are also compared to the
standard MLR, which is found to be more prone to aliasing from non-solar sources than the new
MLR method. The design of the model experiments employed here is more realistic than previous
modeling studies on the impact of aliasing on the detection of the solar signal, as e.g., *Marsh and
Garcia* (2007). The main findings are as follows.

610   – A double-peak profile in both temperature and ozone with maxima in the upper and lower
             stratosphere is diagnosed in the WACCM3.5 simulations forced with all observed forcings.
             This agrees qualitatively well with reanalysis and satellite data.

          – In the tropical lower stratosphere, a substantial portion of the apparent solar-induced increase
             in temperature and ozone is related to volcanic aerosol. This is due to alignment of two major
615   volcanic eruptions (El Chichón and Mt. Pinatubo) with peaks of solar activity during cycles
             21 and 22.

          – Using 45 yr of data, a robust 11 yr solar signal can only be extracted above 10 hPa. At lower
             levels, longer records would be required. This occurs because the solar and volcanic signals
             cannot be adequately separated.

620   – The aliasing issue is ameliorated if windows around El Chichón and Mt. Pinatubo are ex-
             cluded from the analysis (June 1982 to November 1983, and September 1991 to Novem-
             ber 1993). This removal reduces the apparent solar signal in temperature in both modeled and
             observational data. In ozone, further complication is caused by interference with the QBO.

It is plausible that the observed amplitude of the solar-induced increase in the TLS in temperature
625   and ozone (as reported in other studies, 0.8 K in reanalysis (*Frame and Gray*, 2010) and 4 % in
satellite data (*Soukharev and Hood*, 2006)) is overestimated due to issues associated with the MLR
analysis of a too short record that have been explored in this work.

The present results suggest that MLR techniques require the use of longer observational records
for unambigous separation of decadal changes driven by the solar cycle. When regressing reanal-
630   ysis and satellite data, which are available to date (as e.g., MERRA reanalysis data spanning over
26 yr), both windows around El Chichón and Mt. Pinatubo should be removed for more accurate
determination of the solar signal.

Appendix A

635 The standard version of multiple linear regression models takes the following form:

$$Y_t = \sum_{i=1}^{n} \mathbf{X}_{i,t} \beta_i + \varepsilon_t \tag{A1}$$

where Y is the predictand (i.e., the dependent variable); t is the time dimension; $\mathbf{X}$ is a matrix with the basis functions containing n predictors, β are the regression coefficients, and ε is the residual

640 error term.

Multiple linear regression models after Eq. (A1) are commonly used in solar cycle studies. The $\mathbf{X}$ matrix typically contains a set of predictors representing possible sources of variability: a linear trend term for long-term changes due to increases in GHGs and ozone depleting substances, and a set of proxy indices for ENSO, the 11 yr solar cycle, the QBO and volcanic eruptions.

645 Valuable information about the impact of each forcing can be extracted with this method, provided that the correct portion of variance in the predictand time series is fit, along with its relative attribution to each of the predictors. However, this is not the case when the predictors in matrix $\mathbf{X}$ are cross correlated ("multi-collinearity"), and when there is autocorrelation in the predictand time series ("persistence") (*Wilks*, 2011). Spurious correlations with the predictors can arise due to per-

650 sistence in the predictand time series, while multi-collinearity leads to erroneous partitioning of the variance among predictors. Collinearity between the predictors can be significant, especially in relatively short records; an example is the correlation found between the N3.4 index and the 11 yr solar cycle (*Marsh and Garcia*, 2007). Additionally, significant persistence can be found within seasonal time scales in atmospheric field variables, which implies that individual data points in the predictand

655 are not independent.

A common way to circumvent the problem associated with persistence is to treat the residual error term in the regression model as an autoregressive process (*Tiao et al.*, 1990). This method implies correction of both the basis functions in $\mathbf{X}$ and the predictand Y with the autocorrelation coefficient of the residual error term ε estimated from a first application of the regression model.

660 This intermediate step is called "pre-whitening", and its application can be found in numerous papers on the solar signal in the stratosphere (e.g., *Soukharev and Hood*, 2006; *Austin et al.*, 2008; *Frame and Gray*, 2010). Another way to account for autocorrelation is by pre-whitening the predictand Y and predictors $\mathbf{X}$ with the first order autocorrelation coefficient of the original time series of the predictand Y. This is the so-called Box-Jenkins (BJ) methodology (*Box and Jenkins*, 1980).

665 Both pre-whitening techniques were carried out on the output from the WACCM model. It was found that the BJ pre-whitening leads to an autocorrelation function (ACF) that is closer to white noise (not shown), and hence optimal for regression analysis (*Box and Jenkins*, 1980). Hence, the BJ technique was chosen for the analysis of the simulations presented in this paper.

Once the time series have been prewhitened, the regression model equation is carefully assessed

670 upon analysis of the lagged cross correlation structures between the predictors (i.e., the i time series

19

in the **X** matrix), and the predictand Y. This is done to identify the lags that maximize the projection of variance onto the basis functions, improving the fit accuracy.

We performed a preliminary analysis by using both (i) deseasonalized monthly mean, (ii) seasonal mean (3-months averages) and (iii) 3-months running mean anomalies of temperature and ozone. It is found that the use of (ii) seasonal averages filters spurious cross correlation structures showing up at high frequencies (1–2 months) that are related to internal noise rather than a causal relationship. Therefore, seasonal mean anomalies are used in this analysis. The use of seasonal averages is also justified physically. Part of the changes in stratospheric temperature and ozone due to ENSO, QBO and solar cycle are mediated by changes in upwelling rates, especially in the TLS. *Randel et al.* (2002) showed that coherence between temperature and upwelling rates in the TLS is enhanced at seasonal time scales compared to higher frequencies, so that dynamically forced changes in temperature can be better captured with seasonal averages.

In the reference "all forcings" ensemble, the matrix **X** reads as follows

$$\mathbf{X} = \begin{pmatrix} t \\ N3.4 \\ UV \\ u30 \\ u10 \\ SAD \end{pmatrix} \tag{A2}$$

where t is the time dimension in seasons, $N3.4$ is the Niño 3.4 index (the standardized mean sea surface temperature between 5° S–5° N latitude and 120–170° W longitude) for ENSO; UV is the ultraviolet solar radiation flux integrated in the Hartley band (240–270 nm) from the Lean dataset (*Lean et al.*, 2005), and is used as a proxy for the 11 yr solar cycle; $u30$ and $u10$ are the equatorial zonal mean zonal winds at 30 and 10 hPa, which have the quality of being nearly orthogonal proxies for the QBO (*Randel and Wu*, 1996). SAD is the global mean surface area density at 50 hPa (in units $\mu m^2/cm^{-3}$) of sulphate aerosol taken from a combination of different datasets: SAGE I (1979-1981), SAGE II (1984-2005), and SME instruments. Aerosol data before 1979 are constructed based on assumptions of background aerosol (see section 2.5.3.4 of *CCMVal-2*, 2010). Based on SAD, an aerosol mass distribution is assumed in WACCM3.5 for heating rate calculations (*Tilmes et al.*, 2009). Hence, this dataset is the most appropriate proxy for the volcanic forcing in the model simulations.

When using data from the idealized ensembles, the forcings which are kept constant (following table 1) are removed from the **X** matrix. The N3.4 index is excluded in the "fixedSSTs" ensemble, $u10$ and $u30$ are excluded in the "noQBO" ensemble, while the SAD index is excluded in the "noVOLC" ensemble.

20

The first step in the formulation of the regression model is pre-whitening of both sides of Eq. (A1):

$$Y'_{t,z} = Y_{t,z} - \rho_z Y_{t-1,z}$$
$$X'_{t,i,z} = X_{t,i,z} - \rho_z X_{t-1,i,z} \tag{A3}$$

where ρ_z is the autocorrelation coefficient of Y at lag of 1 season and at the level z, i is the forcing index. Equation (A3) is applied at each discrete model level z ranging from 0.1 hPa to 100 hPa. It is found that the use of the autocorrelation at lag 1 is enough to reduce the ACF of Y' to white noise, so that there is no need to use autoregressive models of higher order.

After pre-whitening both forcings and seasonal mean anomalies of temperature and ozone, we calculate the lag τ at which the absolute value of the cross correlation between each predictor i and Y' reaches a maximum value at a given level z.

$$\tau_{i,z} = t \mid\mid r(Y'_{t=0...n,z}, X'_{i,t=0+\tau...n,z}) = \text{MAX} \tag{A4}$$

A separate analysis showed that no significant cross correlation between predictors is introduced by using the 1 yr window. Furthermore, correlations arising at lags larger than the characteristic time scale of each forcing are unlikely to describe a physical link with the dependent variable. This is especially true in the stratosphere, where the responses are not modulated by the ocean.

In the case of the QBO, the indices $u30'$ and $u10'$ are approximately sinusoidal and nearly orthogonal to each other. As such, the use of different lags would introduce correlations between them, and therefore loss of orthogonality. The most accurate fit is obtained by computing the regression coefficient, hence without using any lag in any of the QBO indices. This motivates a different treatment of the QBO in Eq. (A4) compared to the other terms; i.e. by using $\tau_{qbo} = 0$.

An additional complication is posed by the separation of QBO signals from the other sources of variability. We found that the observed zonal wind which is assimilated in the ensembles including a QBO contains significant variations arising from volcanoes, ENSO and solar cycle. For the solar cycle, this result is consistent with the reported modulation of the QBO periodicity by the solar cycle (*Salby and Callaghan*, 2000). We remove the collinearity by computing two filtered QBO indices. For this purpose, we regress the UV, ENSO and SAD indices using their optimal lag τ on zonal mean wind at both 30 and 10 hPa, and take the residual as filtered QBO index, as described by the Eq. (A5).

$$u30^*_{t,z} = u30'_{t,z} - (\beta_{uv} UV'_{t-\tau_{i=uv,z},z} + \beta_{enso} N3.4'_{t-\tau_{i=enso,z},z} + \beta_{volc} SAD'_{t-\tau_{i=volc,z},z})$$
$$u10^*_{t,z} = u10'_{t,z} - (\beta_{uv} UV'_{t-\tau_{i=uv,z},z} + \beta_{enso} N3.4'_{t-\tau_{i=enso,z},z} + \beta_{volc} SAD'_{t-\tau_{i=volc,z},z}) \tag{A5}$$

In this way, $u30^*$ and $u10^*$ are made orthogonal with respect to the other indices, while preserving their mutual orthogonality by excluding any QBO lag. This improves the accuracy of the regression

21

analysis. The two filtered QBO indices, along with the prewhitened and lagged predictors are then used in the target regression model for ozone and temperature.

740

$$Y'_{t,z} = \beta'_{uv} UV'_{t-\tau_{i=uv,z},z} + \beta'_{enso} N3.4'_{t-\tau_{i=enso,z},z} + \beta'_{qbo1} u30^*_{t,z}$$
$$+ \beta'_{qbo2} u10^*_{t,z} + \beta'_{volc} SAD'_{t-\tau_{i=volc,z},z} + e'_{t,z} \tag{A6}$$

For the regression of ozone, the regression coefficients β' are given in relative % units. First,

745   we regress absolute values of tropical mean mixing ratio, and then the percentages are taken on the long-term climatology.

The regression model described by Eq. (A6) is used in the analysis of the reference "all forcings" set. In the idealized sets, the forcings which are kept fixed are excluded from the Eq. (A6).

22

References

Arfeuille, F and Luo, BP and Heckendorn, P and Weisenstein, D. and Sheng, JX and Rozanov, E and Schraner, M and Brönnimann, S and Thomason, LW and Peter, T: Modeling the stratospheric warming following the Mt. Pinatubo eruption: uncertainties in aerosol extinctions, Atmos. Chem. and Phys., 13, 11221-11234, doi:10.5194/acp-13-11221-2013, 2013.

Austin, J., Tourpali, K., Rozanov, E., Akiyoshi, H., Bekki, S., Bodeker, G., Brühl, C. Butchart, N., Chipperfield, M., Deushi, M., Fomichev, V. I., Giorgetta, M. a., Gray, L., Kodera, K., Lott, F., Manzini, E., Marsh, D., Matthes, K., Nagashima, T., Shibata, K., Stolarski, R. S., Struthers, H., and W. Tian: Coupled chemistry climate model simulations of the solar cycle in ozone and temperature, J. Geophys. Res., 113, D11, 1–20, 2008.

Baldwin, M., Gray, L.J., Dunkerton, T.J., Hamilton, K., Haynes, P.H., Randel, W.J., Holton, J.R., Alexander, M.J., Hirota, I., Horinouchi, T., Jones, D.B.A., Kinnersley, J.S., Marquardt, C., Sato, K., and M. Takahashi: The quasi-biennial oscillation, Rev. Geophys., 39, 179-230, 2001.

Bisgaard, S. and M. Kulahci: Time Series Analysis and Forecasting by Example, vol. 815, Wiley, Singapore, 2011.

Box, G., and G. Jenkins: Time Series Analysis. Forecasting and Control, Holder Day, San Francisco, 1980.

Calvo, N., Garcia, R., Randel, W., and Marsh, D.R.: Dynamical mechanism for the increase in tropical up-welling in the lowermost tropical stratosphere during warm enso events, J. Atmos. Sci., 67, 7, 2331–2340, 2010.

CCMVal-2: SPARC CCMVal Report on the Evaluation of Chemistry-Climate Models, edited by: Eyring, V., Shepherd, T.G., and D.W. Waugh, Tech. rep., SPARC Report No. 5, WCRP-132, WMO/TD-1526, World Meteorological Organization, Geneva, 2010.

Chiodo, G., Calvo, N., Marsh, D.R., and Garcia-Herrera, R.: The 11 year solar cycle in transient WACCM3.5 simulations, J. Geophys. Res., 117, D06109, doi:10.1029/2011JD016393, 2012.

Crooks, S., and Gray, L.: Characterization of the 11-year solar signal using a multiple regression analysis of the ERA-40 dataset, J. Climate, 18, doi:10.1175/JCLI-3308.1, 2005.

Diaz, J., Garcia, R., De Castro, F.V., Hernández, E., López, C., and Otero, A.: Effects of extremely hot days on people older than 65 years in seville (Spain) from 1986 to 1997, Int. J. Biometeorology, 46, 3, 145-149, 2002.

Diaz, J., Jordán, A., García, R., López, C., Alberdi, J., Hernández, E., and Otero, A.: Heat waves in madrid 1986–1997: effects on the health of the elderly, Int. Arch. Occ. Env. Health, *75*(3), 163–170, 2002.

Eyring, V., Cionni, I., Bodeker, G.E., Charlton-Perez, A.J., Kinnison, D.E., Scinocca, J.F., Waugh, D.W., Akiyoshi, H., Bekki, S., Chipperfieldm M.P., and others: Multi-model assessment of stratospheric ozone return dates and ozone recovery in CCMVal-2 models, Atmos. Chem. Phys., 10, 19, 11659-11710, 2010.

Calvo-Fernández, N. C., Garcia-Herrera, R., Puyol, D.G., Hernandez, E., GarcÍa, R., Gimeno, L., Ribera, P.: Analysis of the enso signal in tropospheric and stratospheric temperatures observed by msu, 1979-2000, J. Climate, 17, 20, 3934-3946, 2004.

Frame, T., and Gray, L-J.: The 11-year solar cycle in era-40 data: an update to 2008, J. Climate, 23, 2213-2222, 2010.

Garcia, R., Marsh, D.R., Kinnison, D., Boville, B., and Sassi F.: Simulation of secular trends in the middle

23

atmosphere, 1950–2003, J. Geophys. Res., 112, D09301, doi:10.1029/2006JD007485, 2007.

Gray, L., Beer, J., Geller, M., Haigh, J.D., Lockwood, M., Matthes, K., Cubasch, U., Fleitmann, D., Harrison, G., Hood, L., Luterbacher, J., Meehl, G.A., Shindell, D., Van Geel, B., and White, W.: Solar influences on climate, Rev. Geophys., 48, RG4001, 1-53, 2010.

805   Haigh, J., and Blackburn, M.: Solar influences on dynamical coupling between the stratosphere and troposphere, Space Sci. Reviews, 125, 331–344, 2006.

Hood, L.: The solar cycle variation of total ozone: Dynamical forcing in the lower stratosphere, J. Geophys. Res., 102, D1, 1355-1370, 1997.

Hood, L., and Soukharev, B.: Quasi-decadal variability of the tropical lower stratosphere: The role of extrat-
810   ropical wave forcing, J. Atmos. Sci., 60, 19, 2389-2403, 2003.

Hood, L., Soukharev, B., McCormack, J.: Decadal variability of the tropical stratosphere: Secondary influence of the el niño–southern oscillation, J. Geophys. Res., 115, D11113, doi:10.1029/2009JD012291, 2010.

Hurrell, J. W., J. J. Hack, D. Shea, J. M. Caron, and J. Rosinski: A new sea surface temperature and sea ice boundary dataset for the community atmosphere model, J. Climate, 21, 19, 5145–5153, 2008.

815   Kodera, K., and Kuroda, Y.: Dynamical response to the solar cycle, J. Geophys. Res., 107,D24, 4749.

Lean, J., Rottman, G., Harder, J., and Kopp, G.: Sorce contributions to new understanding of global change and solar variability, The Solar Radiation and Climate Experiment (SORCE), Sol. Phys., 230, 27–53, 2005.

Lee, H., and Smith, A.: Simulation of the combined effects of solar cycle, quasi-biennial oscillation, and volcanic forcing on stratospheric ozone changes in recent decades, J. Geophys. Res., 108, D24049, doi:10.1029/2001JD001503, 2003.
820

Marsh, D.R., and Garcia, R.: Attribution of decadal variability in lower-stratospheric tropical ozone, Geophys. Res. Lett., 34, L21807, doi:10.1029/2007GL030935, 2007.

Matthes, K., D. Marsh, R. Garcia, D. Kinnison, F. Sassi, and S. Walters: Role of the QBO in modulating the influence of the 11 year solar cycle on the atmosphere using constant forcings, J. Geophys. Res., 115,
825   D18110, doi:10.1029/2009JD013020, 2010.

Meehl, G., J. Arblaster, K. Matthes, F. Sassi, and H. van Loon: Amplifying the Pacific climate system response to a small 11-year solar cycle forcing, Sci., 325, 5944), 1114–1118, 2009.

Pap, J., and P. Fox: Solar variability and its effects on climate, Washington DC American Geophysical Union Geophysical Monograph Series, 141, 2003.

830   Randel, W. J., F. Wu, J. Russell, J. Waters, and L. Froidevaux: Ozone and temperature changes in the strato-sphere following the eruption of mount pinatubo, J. Geophys. Res., 100, D8, 16753–16764, 1995.

Randel, W., and F. Wu: Isolation of the Ozone QBO in SAGE 2 Data by Singular-Value Decomposition, J. Atmos. Sci., 53, 17, 2546-2560, 1996.

Randel, W. J., R. R. Garcia, and F. Wu: Time-dependent upwelling in the tropical lower stratosphere estimated
835   from the zonal-mean momentum budget, J. Atmos. Sci., 59, 13, 2141–2152, 2002.

Randel, W., and F. Wu: A stratospheric ozone profile data set for 1979–2005: Variability, trends, and compar-isons with column ozone data, J. Geophys. Res, 112, D06313, doi:10.1029/2006JD007339, 2007.

Randel, W., R. Garcia, N. Calvo, and D. Marsh: ENSO influence on zonal mean temperature and ozone in the tropical lower stratosphere, Geophys. Res. Lett, 36, L15822, doi:10.1029/2009GL039343, 2009.

840   Randel, W. J., and K.P. Shine, J. Austin, J. Barnett, C. Claud, N.P. Gillett, P. Keckhut, U. Langematz, R. Lin,

Long, C., Mears, C., Miller, A., Nash, J., Seidel, D.J., Thompson, D.W.J., Wu, F., and S. Yoden: An update of observed stratospheric temperature trends, J. Geophys. Res., 114, (D2), 107, 2009.

Rienecker, M. M., Michele M and Suarez, Max J and Gelaro, Ronald and Todling, Ricardo and Bacmeister, Julio and Liu, Emily and Bosilovich, Michael G and Schubert, Siegfried D and Takacs, Lawrence and Kim, Gi-Kong and others: Merra: Nasa's modern-era retrospective analysis for research and applications, J. Climate, *24*(14), 3624–3648, 2011.

Robock, A.: Volcanic eruptions and climate, Rev. Geophys., *38*(2), 191–219, 2000.

Salby, M., and P. Callaghan: Connection between the solar cycle and the qbo: The missing link*, J. Climate, *13*(14), 2652–2662, 2000.

Schmidt, H., G. Brasseur, and M. Giorgetta: Solar cycle signal in a general circulation and chemistry model with internally generated quasi biennial oscillation, J. Geophys. Res., *115*(D00I14), 16, 2010.

Smith, A., and K. Matthes: Decadal-scale periodicities in the stratosphere associated with the solar cycle and the QBO, J. Geophys. Res., *113*, D05,311, 2008.

Soukharev, B., and L. Hood: Solar cycle variation of stratospheric ozone: Multiple regression analysis of long-term satellite data sets and comparisons with models, J. Geophys. Res., *111*(D20314), 2006.

Thomason, L., L. Poole, and T. Deshler: A global climatology of stratospheric aerosol surface area density deduced from stratospheric aerosol and gas experiment ii measurements: 1984-1994, J. Geophys. Res., *102*(D7), 8967-8976, 1997.

Tiao, G., G. Reinsel, D. Xu, J. Pedrick, X. Zhu, A. Miller, J. DeLuisi, C. Mateer, and D. Wuebbles: Effects of autocorrelation and temporal sampling schemes on estimates of trend and spatial correlation, J. Geophys. Res., *95*(D12), 20,507–20,517, 1990.

Tilmes, S., R. Garcia, D. Kinnison, A. Gettelman, and P. Rasch: Impact of geoengineered aerosols on the troposphere and stratosphere, J. Geophys. Res., *114*(D12305), 2009.

Wilks, D. S. (2011), Statistical methods in the atmospheric sciences, vol. 100, Academic press, 2011.

Tables

name	SSTs	QBO	volcanoes	solar
"all forcings" (2)	observed (*Hurrell et al.*, 2008)	assimilated (*Matthes et al.*, 2010)	SAGE II (*Thomason et al.*, 1997)	(*Lean et al.*, 2005)
"fixedSSTs"(2)	climatological	assimilated (*Matthes et al.*, 2010)	SAGE II (*Thomason et al.*, 1997)	(*Lean et al.*, 2005)
"noQBO" (2)	observed (*Hurrell et al.*, 2008)	none (weak east)	SAGE II (*Thomason et al.*, 1997)	(*Lean et al.*, 2005)
"noVOLC" (2)	observed (*Hurrell et al.*, 2008)	assimilated (*Matthes et al.*, 2010)	climatological	(*Lean et al.*, 2005)

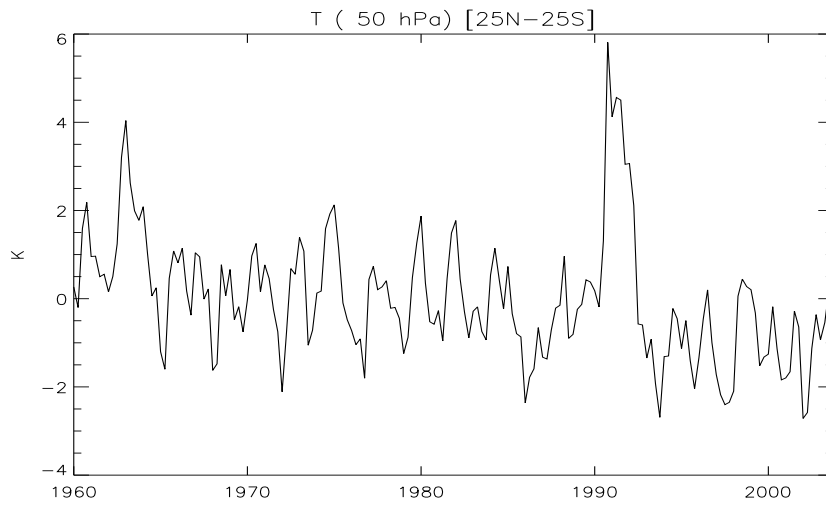**Table 1.** Table of the performed WACCM3.5 ensembles.

Figures

25

Fig. 1. Time series of the simulated seasonal mean temperature anomalies at 50 hPa, averaged over the tropics [25°N-25°S] in the reference "all forcings" set. Units K
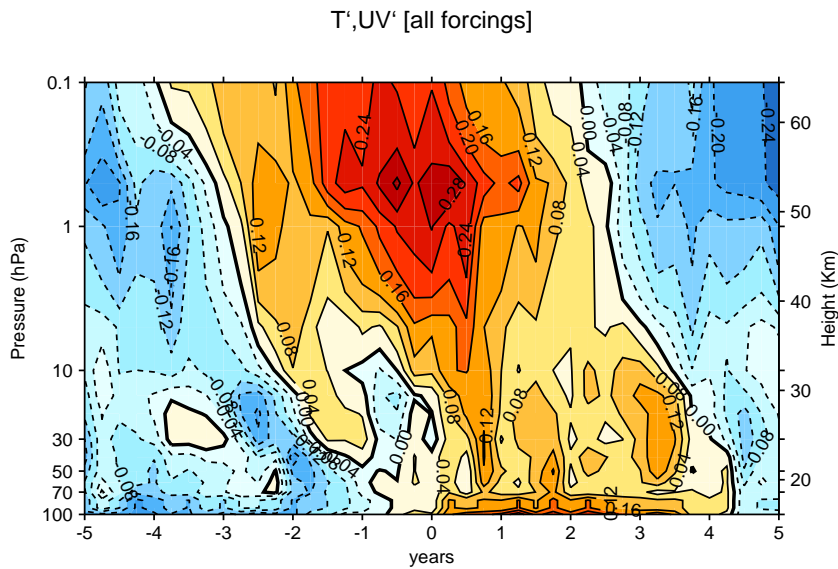

Fig. 2. Lag correlation between the tropical average [25°N-25°S] prewhitened seasonal mean temperature from the "all forcings" case and the UV radiation index. Positive lags mean that UV predictor leads temperature changes. Solid contours and red colors denote positive correlations, while dashed contours and blue colors indicate negative correlations. Contours are drawn every 0.04.

26
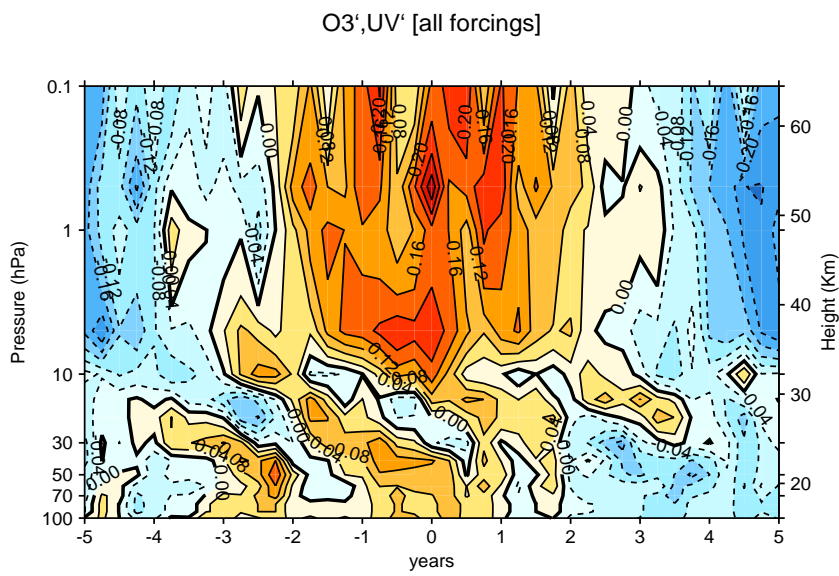
Fig. 3. As in Figure 2, for tropical mean zonal mean ozone from the "all forcings" case.
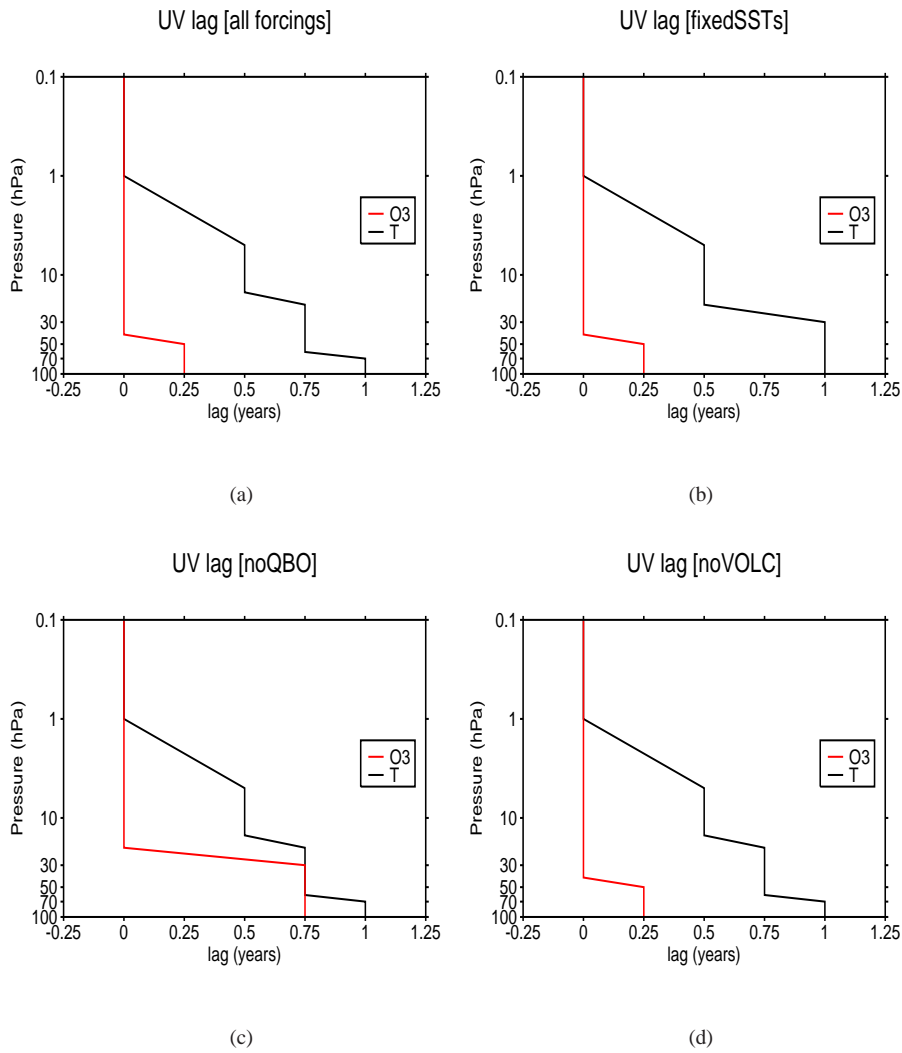
Fig. 4. Vertical profile of the lag that maximises the absolute value of the correlation (in the 0-1 years window) between UV radiation and prewhitened seasonal mean temperature (black) and ozone (red); from (a) the "all forcings", (b) "fixedSSTs" , (c) "noQBO", and (d) "noVOLC" sets. The values are introduced as $\tau_{i=uv}$ in Eq. (A6) for regression of tropical average temperature and ozone.
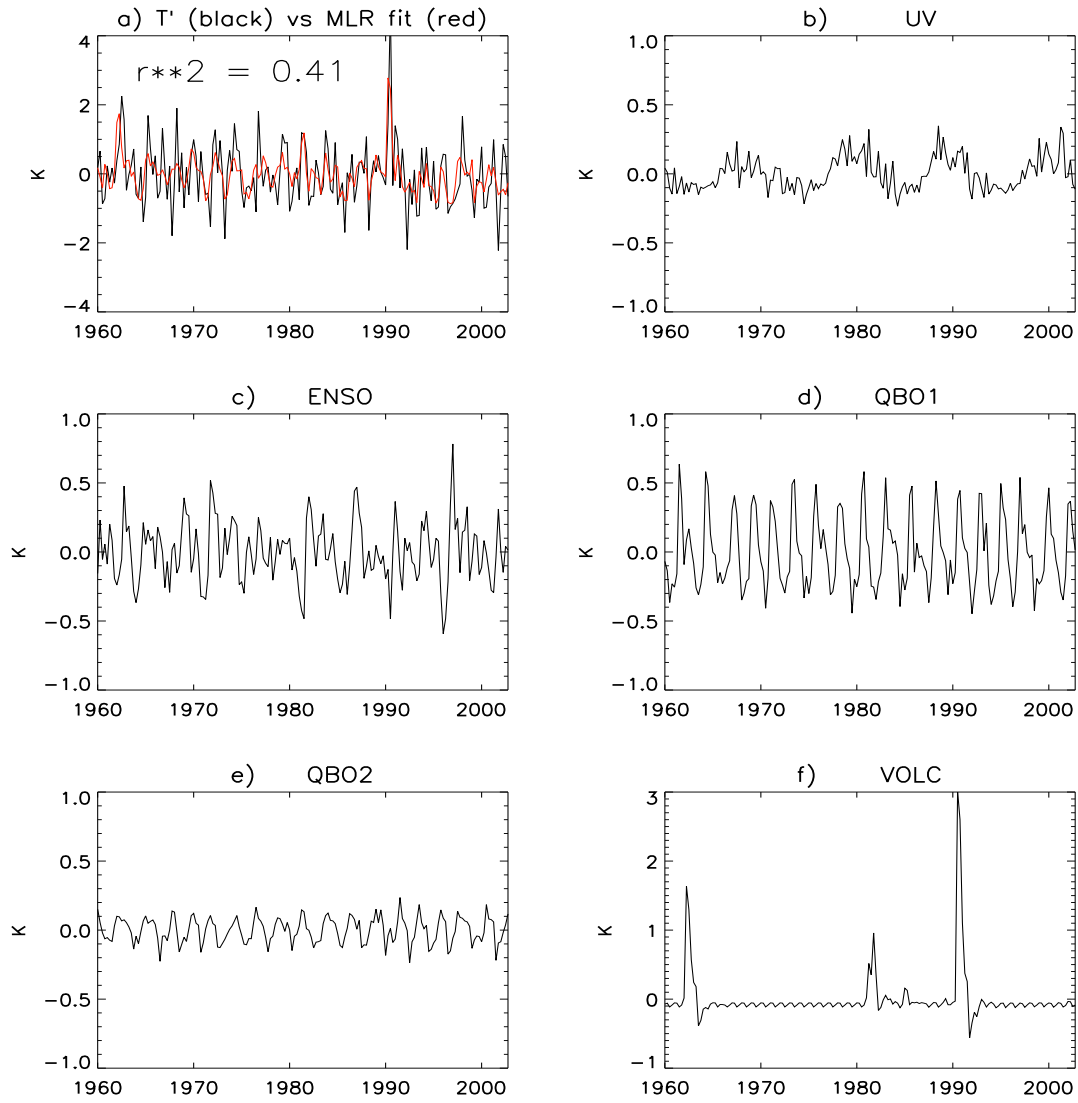
Fig. 5. (a) Time series of tropical average seasonal mean zonal mean temperature anomalies at 50 hPa after pre-whitening (black), along with the regression fit from Eq. (A6) (red); (b-f) Contribution of each of the terms on the right hand side of Eq. (A6) to the regression fit.
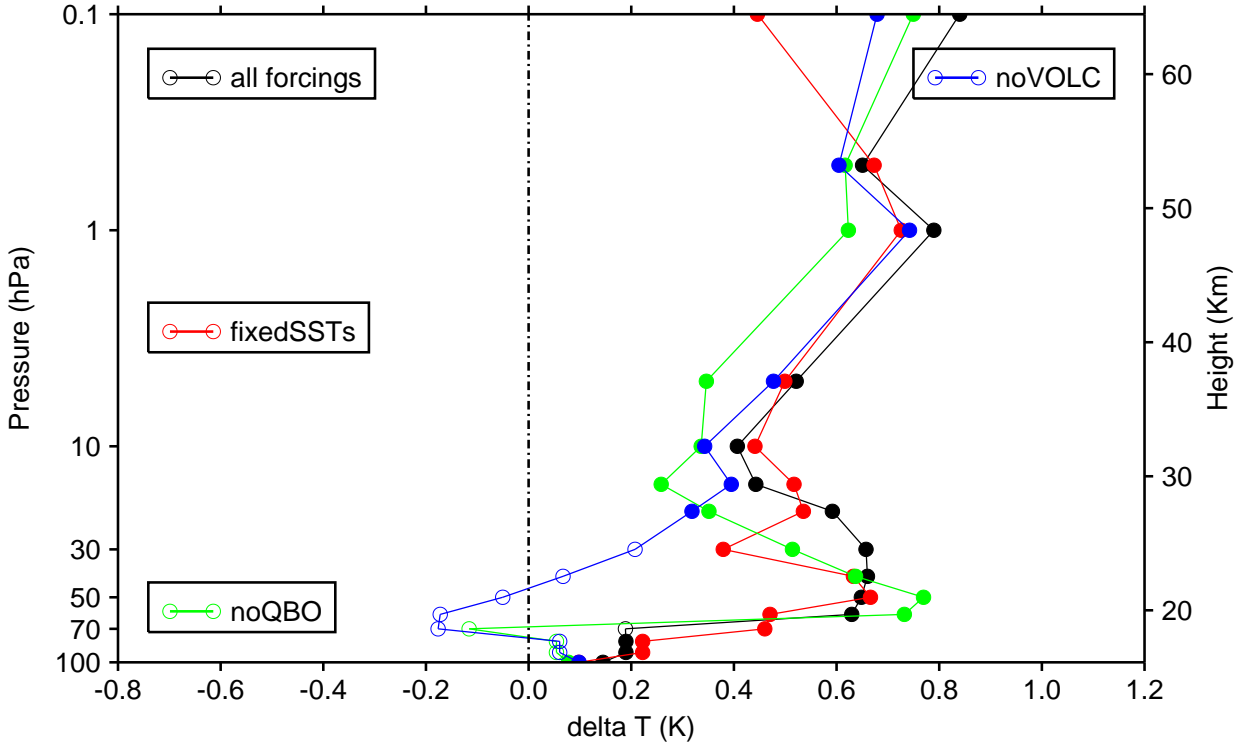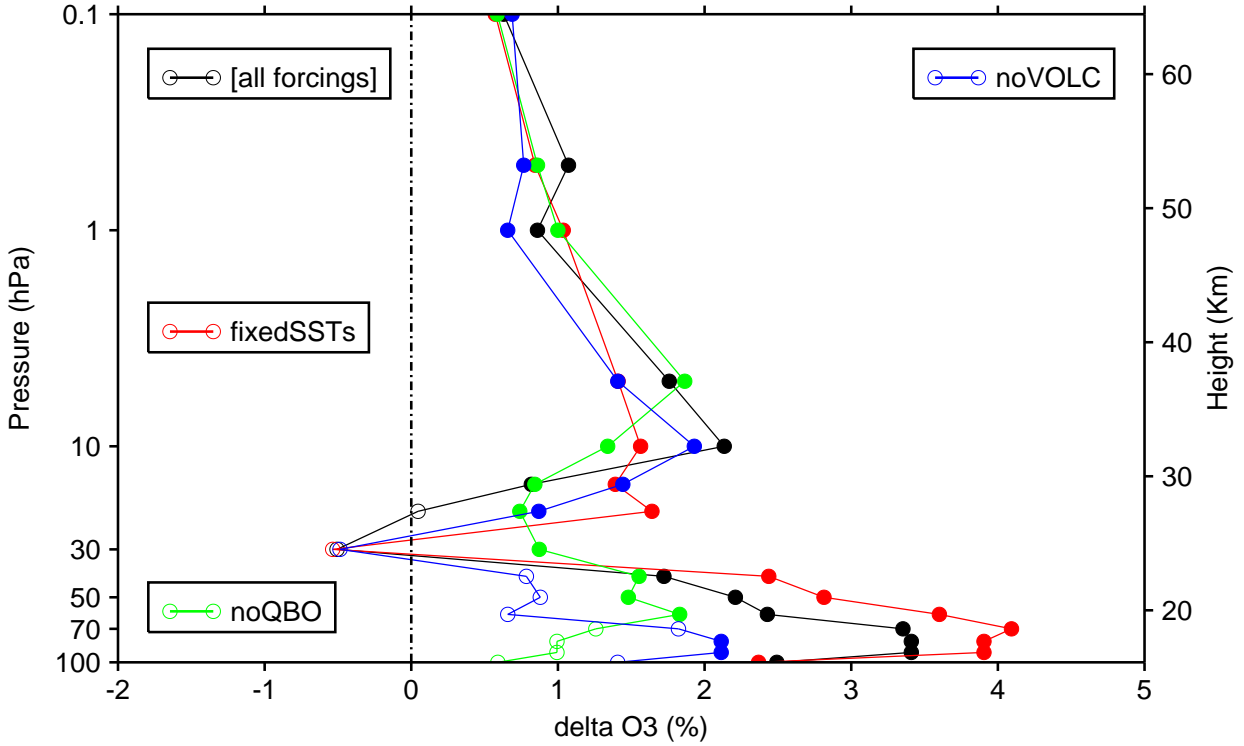
Fig. 6. Solar signal in tropical average zonal mean temperature, estimated as the UV regression coefficient (β'_{UV} in Eq. (A6)) multiplied by 0.175, which represents the 2σ variation of the UV index used in the MLR. Delta K units denote the relative solar cycle peak to trough change in Kelvin. Filled dots indicate that the derived regression coefficients are significantly different from 0 at the 2σ significance level. The lags used for the UV index in each experiment set is the black line shown in Figure 4.
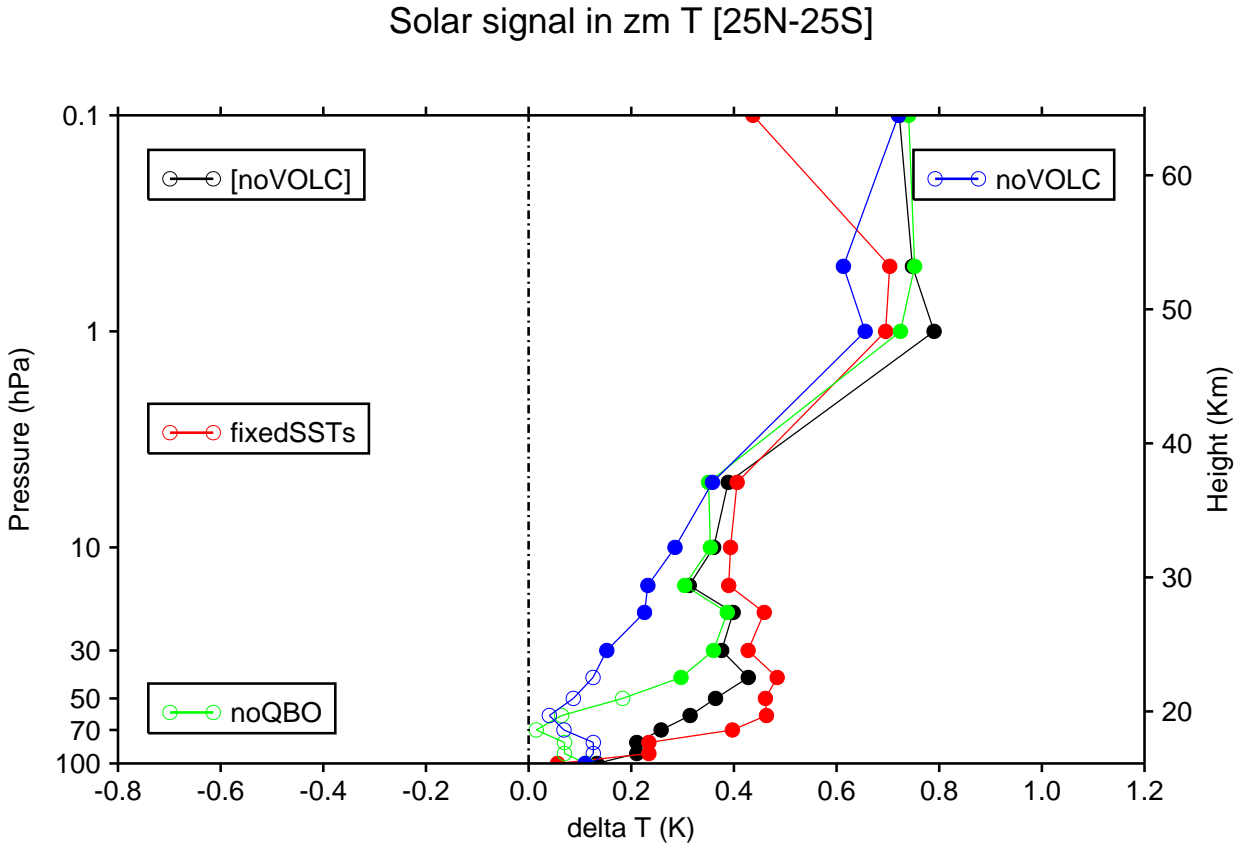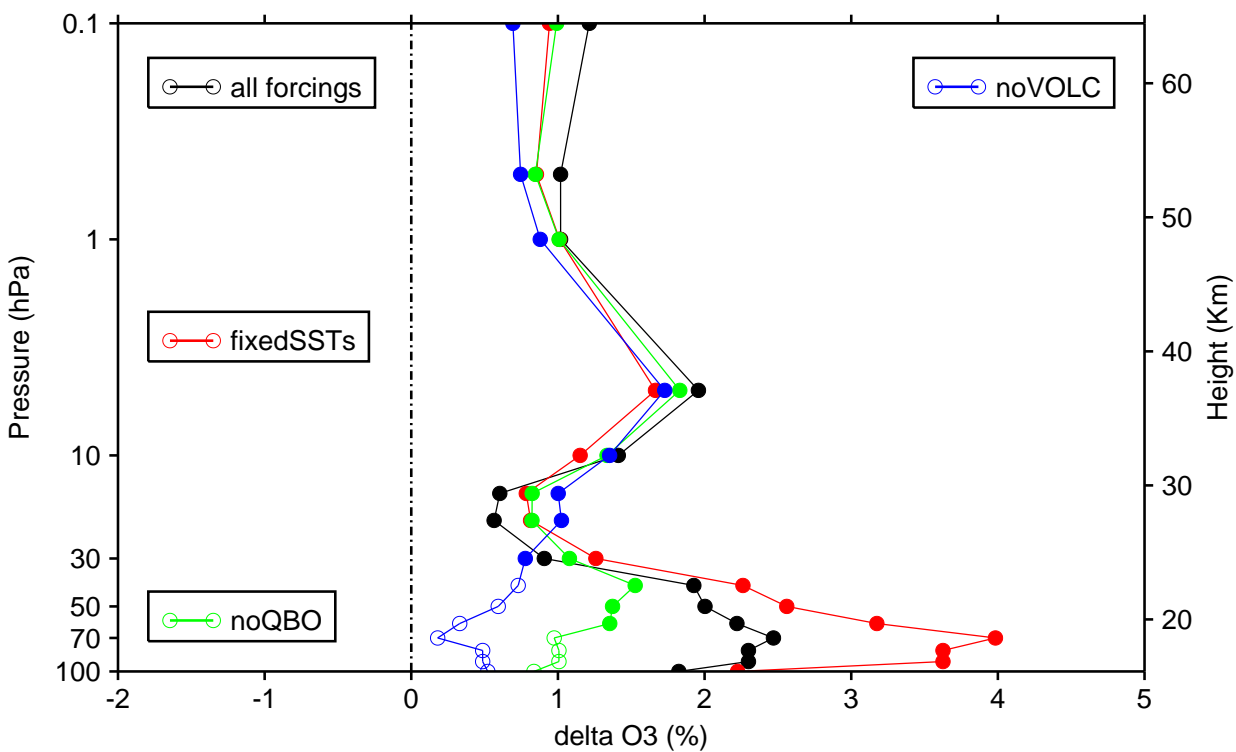
Fig. 7. As in Fig. 6, calculated as the UV regression coefficient from a standard MLR (β_{uv} in Eq. (A1)) multiplied by 0.175, which represents the 2σ variation of the UV index used in the MLR.

Solar signal in zm O3 [25N-25S]

Fig. 8. Solar signal in tropical average zonal mean ozone, estimated as the UV regression coefficient (β'_{UV} in Eq. (A6)) multiplied by 0.175, which represents the 2σ variation of the UV index used in the MLR. Delta % units denote the relative solar cycle peak to trough change in % (i.e., relative change in mixing ratio). Filled dots indicate that the derived regression coefficients are significantly different from 0 at the 2σ significance level. The lags used for the UV index in each experiment set is the red line shown in Figure 4.

Solar signal in zm O3 [25N-25S]

Fig. 9. As in Fig. 8, calculated as the UV regression coefficient from a standard MLR (β_{uv} in Eq. (A1)) multiplied by 0.175, which represents the 2σ variation of the UV index used in the MLR.
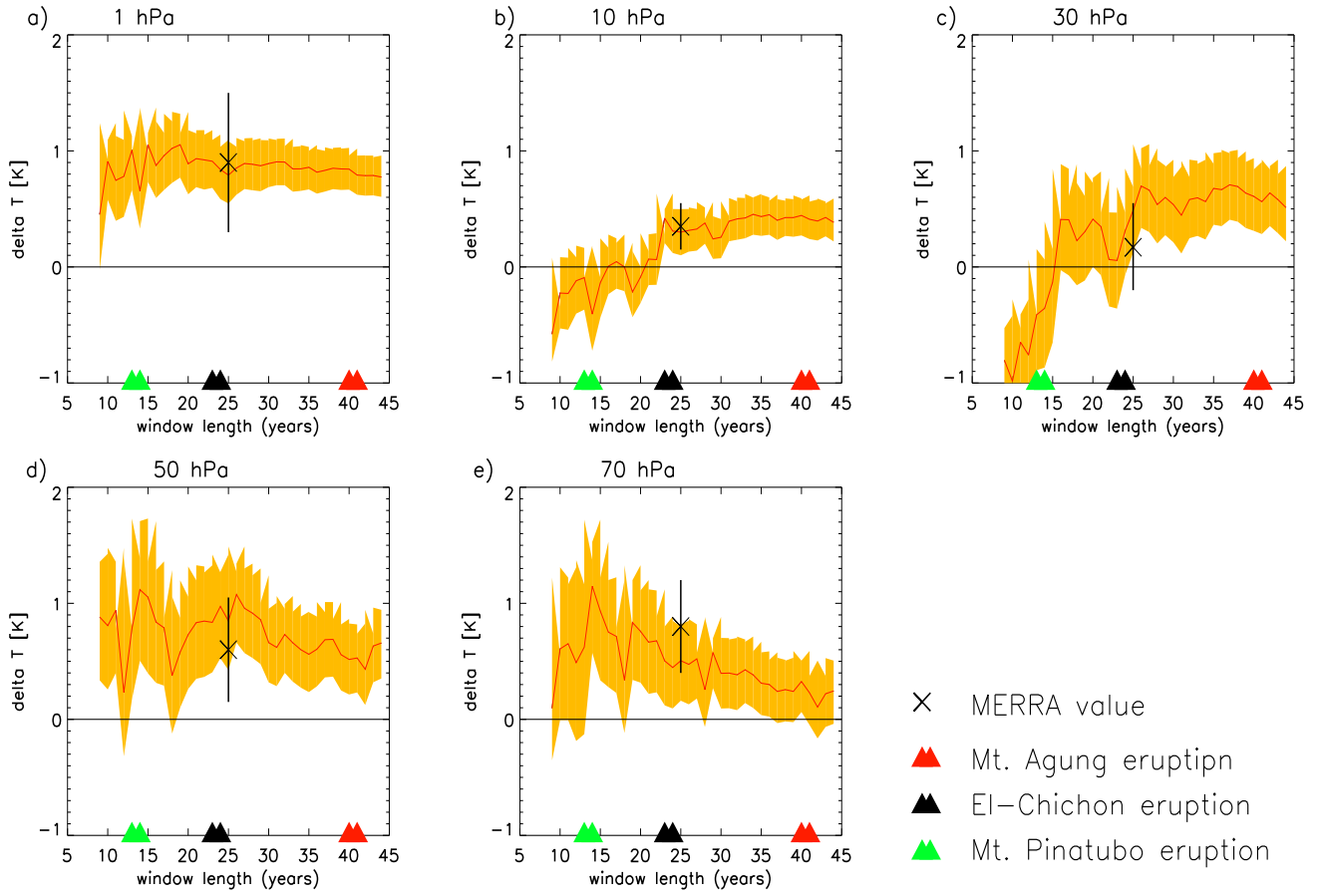
Fig. 10. UV regression coefficient (β'_{UV} in Eq. (A6)) in tropical mean zonal mean temperature (red line) along with the 2σ uncertainty (yellow shading) from the "all forcings" case, plotted as a function of the window used (in years). The endpoint of the window is the last available year in the ensembles, i.e., 2004. Results are shown for (a) 1 hPa, (b) 10 hPa, (c) 30 hPa, (d) 50 hPa, and (e) 70 hPa. Crosses show the values obtained from MERRA reanalysis at 30, 50 and 70 hPa using the window overlapping the simulation period (1979-2004). Units K.
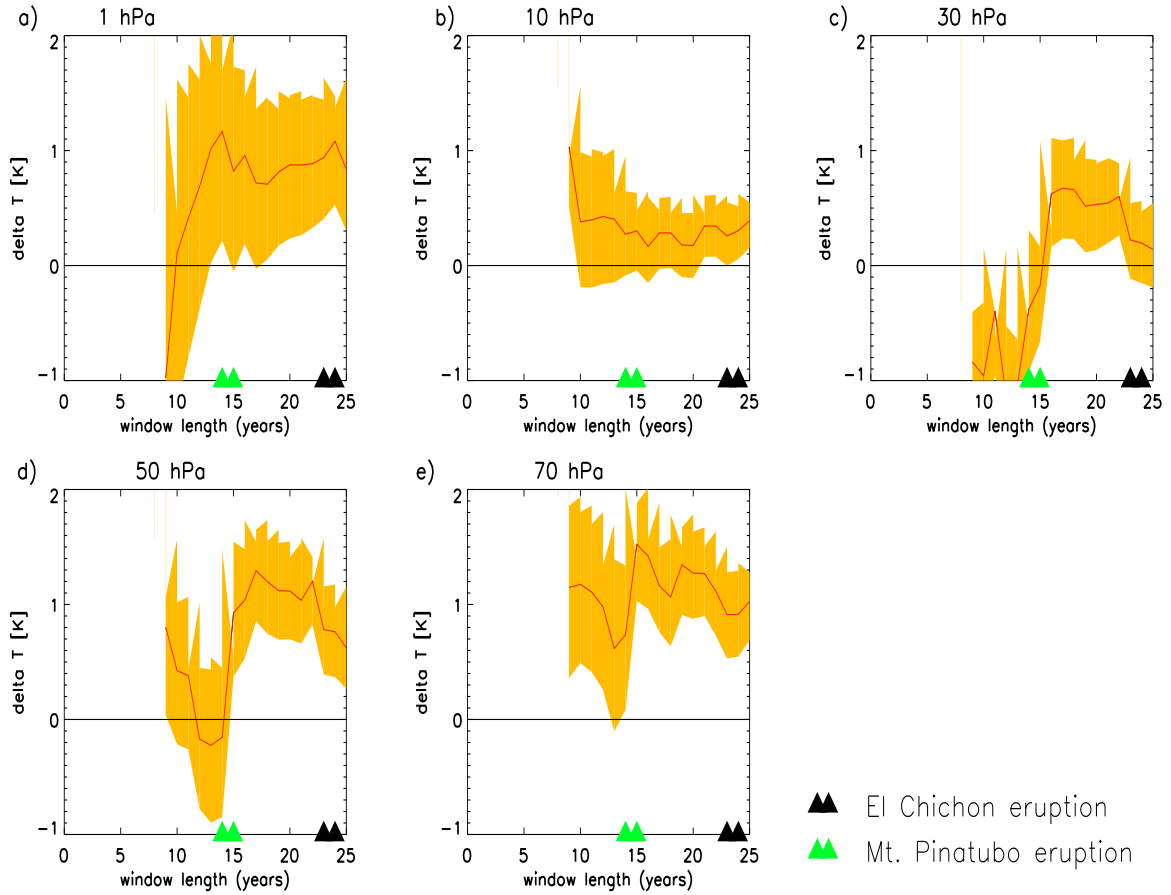
Fig. 11. UV regression coefficient (β'_{UV} in Eq. (A6)) in tropical average zonal mean temperature from MERRA reanalysis, displayed as a function of the window used, which is 26 yr long. Note that the signal has been computed with the same regression technique as in WACCM. The endpoint of the window is the last available year in the WACCM simulations, i.e., 2004. Units K.
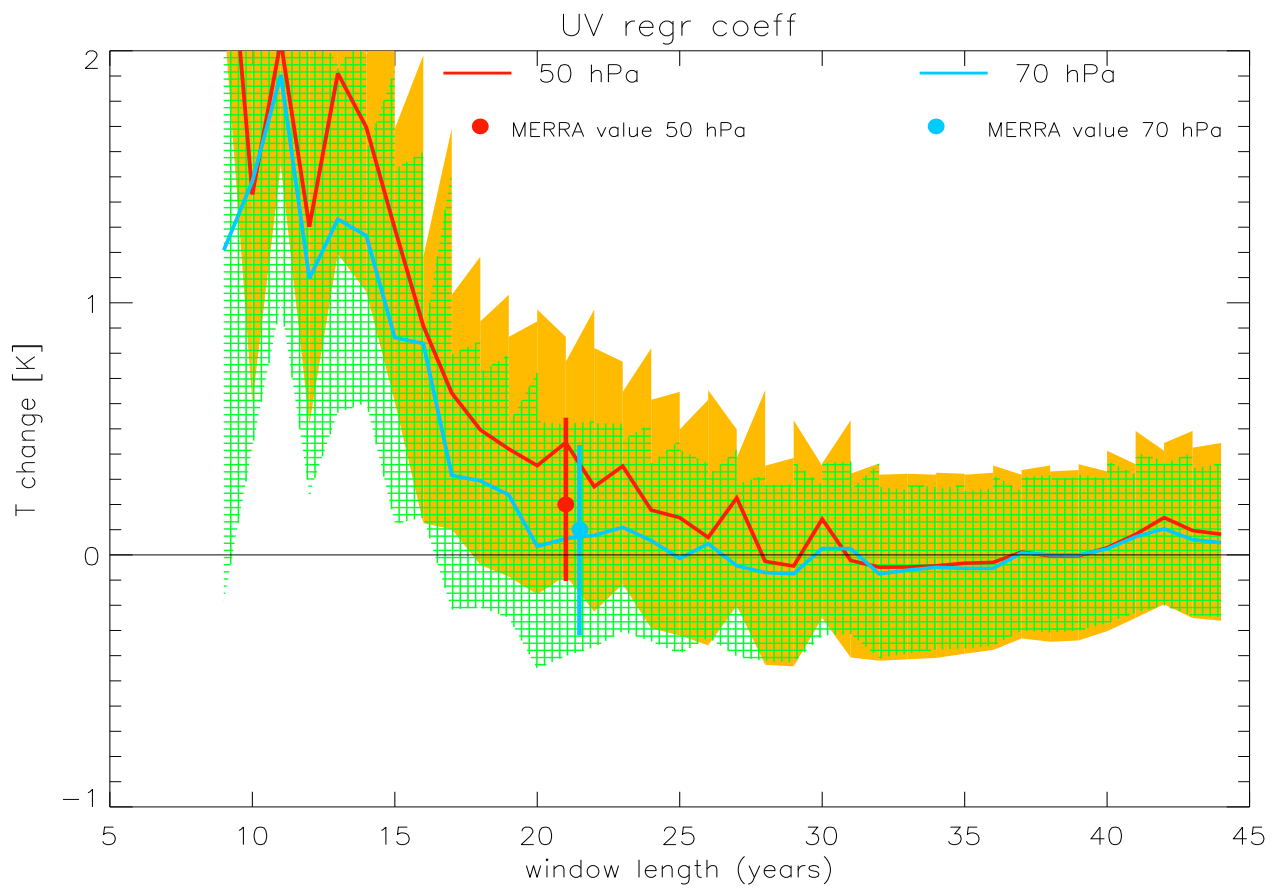
Fig. 12. UV regression coefficient in tropical mean zonal mean temperature from the "all forcings" case, obtained when omitting post El Chichón and Mt. Pinatubo data (see exact dates indicated in the text), plotted as a function of the years included in the window. The endpoint of the window is the last available year in the ensembles, i.e., 2004. Results are shown for the 50 hPa (red) and 70 hPa (blue) levels, along with the 2σ uncertainty (yellow for 50 hPa, and green for 70 hPa). Dots indicate the values obtained from MERRA reanalysis, along with the 2σ uncertainty. Units K.
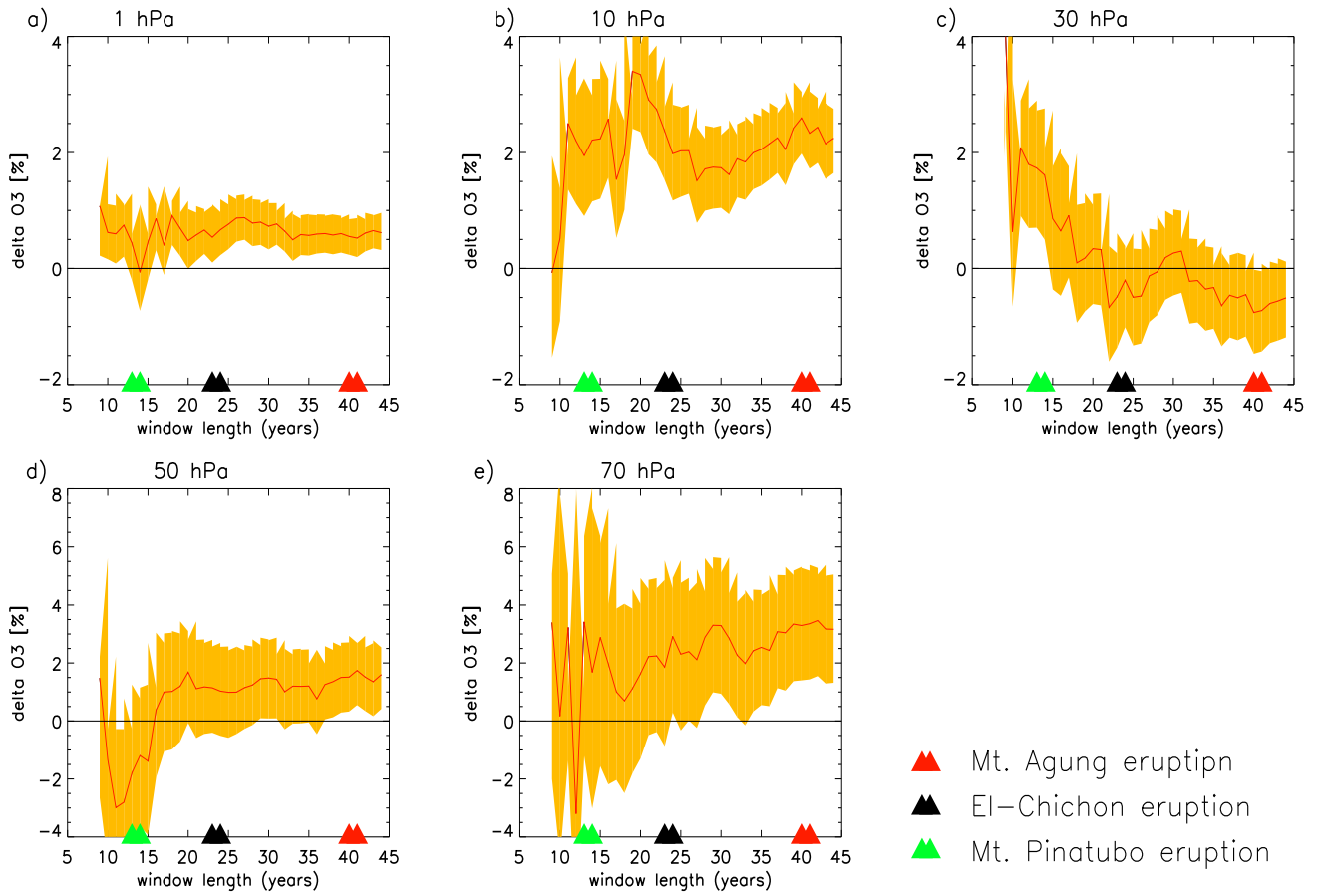
Fig. 13. As in Figure 10, for tropical mean zonal mean ozone. Units % (i.e., relative change in mixing ratio).
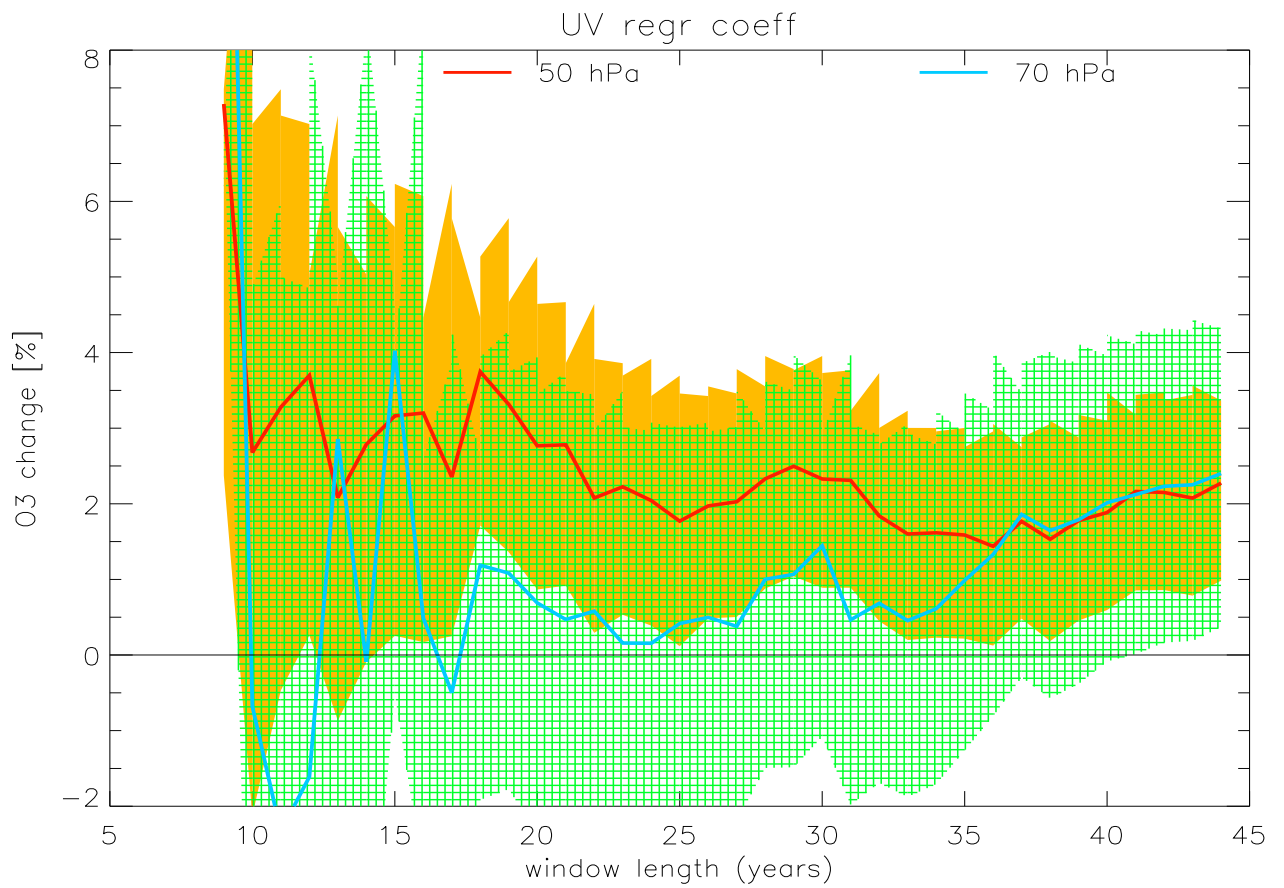
Fig. 14. UV regression coefficient in zonal mean ozone from the "all forcings" case, omitting the post El Chichón and Mt. Pinatubo data (June 1982 to November 1983, and September 1991 to November 1993), plotted as a function of the window used (in years) for 50 hPa (red) and 70 hPa (blue), along with the 2σ uncertainty (yellow shading for 50 hPa, and green shading for 70 hPa). The endpoint of the window is the last available year in the ensembles, i.e., 2004. Units %.